AN INNOVATIVE ISOLATION DEVICE FOR ASEISMIC DESIGN

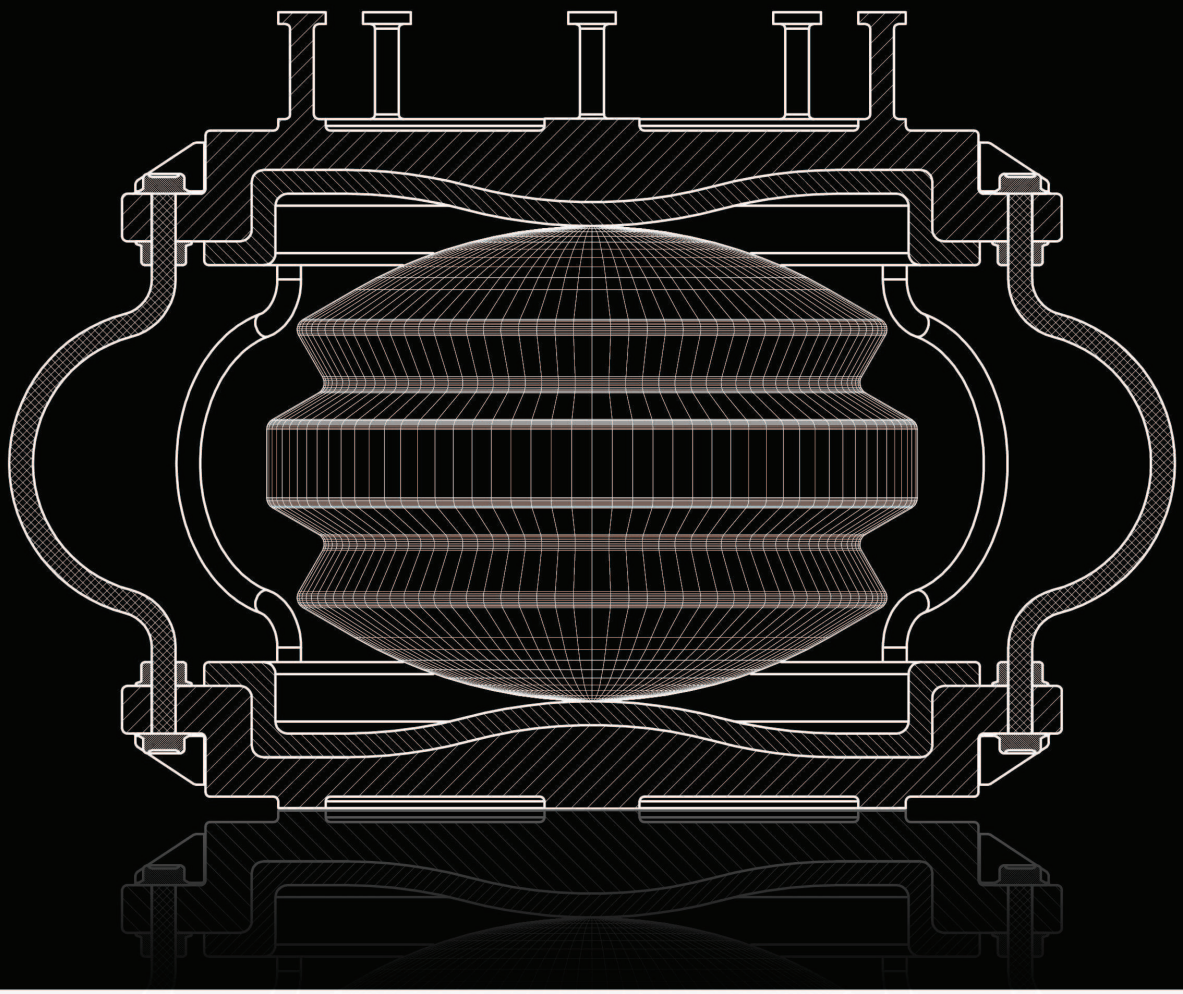

Mohammed Ismail Abdel-Kareem Moustafa

Doctoral Thesis

Barcelona, October 2009

6 Isolation of light-to-moderate mass buildings

6.1 Introduction

Designing earthquake-resistant low- to medium-rise structures is problematic in that their fundamental frequency of vibration is in the range of frequencies where earthquake energy is the strongest. Thus, the building acts as an amplifier of the ground vibrations, with the floor accelerations increasing over the height of the building. Ultimately, the seismic design should reduce the accelerations in buildings to below the level of the ground accelerations. To do this the building must be flexible. For a low- or medium-rise building, the necessary flexibility can only be achieved by using seismic isolation at the foundation level to shift the structural period away from the period range having the most of earthquake energy, while leaving the structure to undergo almost a rigid body motion [223, 248].

Although the first patents for seismic isolation were in the 1800's, it was the 1970's before seismic isolation moved into the mainstream of structural engineering. The lead rubber bearing (LRB) was invented in the 1970's, [374, 375, 433] and this allowed the flexibility and damping to be included in a single unit. In the early 1980's, developments in rubber technology lead to new rubber compounds which were termed high damping rubber (HDR) [117]. Both LRB and HDR isolation systems have design restrictions on the height/width and deformation/height ratios. These restrictions enforce a minimum limit of the provided horizontal flexibility. If this limit is exceeded, the bearing stability is drastically affected. Certainly, this lowers the bearing aptitude to isolate low-mass structures, as low mass has to be associated with low stiffness to achieve

the required isolation period.

Flat sliding bearings were not used alone as the isolation systems as they lack a restoring force mechanism. The development of the friction pendulum system (FPS) [12] provided the sliding bearings with a gravitational restoring force but, unfortunately, on the account of fixed vibration period of the FPS [331]. Moreover, the high cost of the articulated slider in FPS hinders its economic use for light buildings. This usually makes the isolators more expensive with respect to the total cost of light- to moderate mass structures.

Although many other systems have been promulgated, based on rollers, springs, cables etc, the market for base isolation now is mainly distributed among variations of LRBs, HDR bearings, flat sliding bearings and FPS. There have been systems proposed to isolate light buildings. However, the fact remains that there are few instances of successful isolation of light structures.

In this chapter, the RNC isolation bearing is intended to protect light- to moderate mass structures from seismic hazards. For such structures, their lower mass has to be associated with lower isolator stiffness to achieve effective isolation. This condition could not be fulfilled by many of the present day isolators, but the rolling-based RNC isolator can fulfill such condition. The performance of the RNC is numerically investigated for a wide range of structural, isolator and ground motion characteristics.

6.2 The used RNC isolator type

The RNC–c isolator, that is more suitable for light- to moderate mass structures, is designed and used in this chapter. This RNC type is shown in Fig. 3.1. For the designed RNC–c isolator, the horizontal and vertical distances between the furthermost points are 2.48 m and 1.40 m, respectively. The isolator dimensions are chosen to allow for 53 cm as a maximum rolling displacement, beyond which the buffer mechanism stops the isolated structure with minimal shock.

6.3 Mechanical characteristics

Following the mechanical characterization scheme described in Section 4.2, the designed RNC–c isolator used in this chapter has the following mechanical characteristics:

- Maximum vertical load capacity = 600 kN.
- Pre-yield stiffness of 12246 kN m^{-1}.
- Post-yield stiffness of 144 kN m^{-1}.

- Yield displacement of 1.27 cm.
- Yield force of 159 kN.
- Characteristic strength of 157 kN.

Further, three different designs of each RNC–c isolator, ranging from stiff (sets I) to very flexible (sets III) designs, are evaluated in this chapter in order to draw relatively general conclusions about the performance of the RNC–c isolator. The maximum vertical load capacity per bearing is 600 kN. Table 6.1 gives the basic mechanical characteristics of such designs. These characteristics have been also obtained following the scheme given in Section 4.2.

Isolator Set	Isolator Period (T_b)	Elastic Stiffness (k_e)	Post-yield Stiffness (k_b)	Yield Strength (f_y)	Characteristic Strength (Q)
I	2.932 sec	712.387	27.096	9.648	9.525
II	4.416 sec	356.194	13.550	4.824	4.762
III	5.863 sec	178.097	6.775	2.412	2.381

Table 6.1: Characteristics of different RNC–c isolator sets used in study, ton-m units.

6.4 Hysteretic modeling

The characterization described in Chapter 4 has shown that the RNC isolator exhibits a hysteretic behavior, as shown in Fig. 4.7. The objective of this section is to obtain an input-output mathematical model to describe in a reasonable and manageable form the force-displacement relationship exhibited by the RNC–c isolator using the Bouc-Wen model of smooth hysteresis, described in Section 4.5. The normalized form of the Bouc-Wen model is used in this chapter. Such form of the model is defined in Section 4.5.4.

6.4.1 Bouc-Wen model parameters estimation

The normalized Bouc-Wen form provides an exact and explicit expression for the hysteretic limit cycle [200]. Therefore, by using a periodic input signal $x(t)$ along with analytical description of the limit cycle, a robust parametric nonlinear, nonrecursive identification method or the normalized Bouc-Wen model was presented [201, 194]. This method provides exact values of the model parameters in the absence of disturbances, and gives a guaranteed relative error between the estimated parameters and the true ones in the presence of the

perturbations. This identification method is used in this chapter, leading to the following parameters of the normalized Bouc-Wen model:

$$\kappa_{\mathrm{x}} = 19.315; \quad \kappa_{\mathrm{w}} = 16.227; \quad \rho = 55.641; \quad \sigma = 1.022; \quad n = 2.162$$

An efficiency measure of the identified parameters is carried out through the model validation.

In Fig. 6.1, the measured output restoring force of the isolator is plotted against the calculated one via the identified normalized Bouc-Wen model. The good matching shows that the Bouc-Wen model is able to capture the nonlinear hysteretic behavior of the proposed isolator.

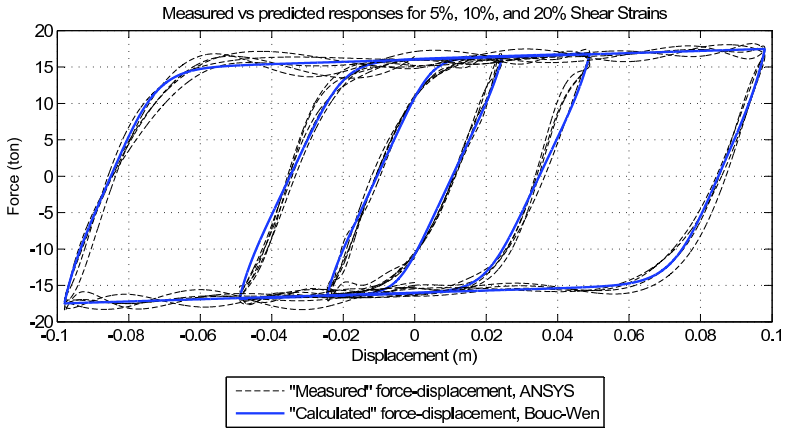

Figure 6.1: Measured vs calculated restoring force for 5%, 10% and 20% shear strains

6.4.2 Seismic verification of the Bouc-Wen model

To further check the validity of the identified parameters, an actual random seismic displacement (El-Centro) signal is input to the ANSYS and the Bouc-Wen models. Then, the discrepancy between the measured and predicted outputs, F_{m} and F_{b}, is quantified using the L_1 and L_∞-norms and the corresponding relative errors ε as expressed in (4.19).

Fig. 6.2(a) shows the input displacement of El-Centro earthquake record to the ANSYS and Bouc-Wen models. As shown in Fig. 6.2(b) and the relative errors ε_1 and ε_∞, the hysteretic Bouc-Wen model can be seen as a very powerful replacement of the experimental prototype for more case studies using the RNC isolator. This is asserted by the relatively small error percentages ($\varepsilon_1 = 5.70\%$ and $\varepsilon_\infty = 3.15\%$) and the close match of both measured and predicted output curves observed in Fig. 6.2(b).

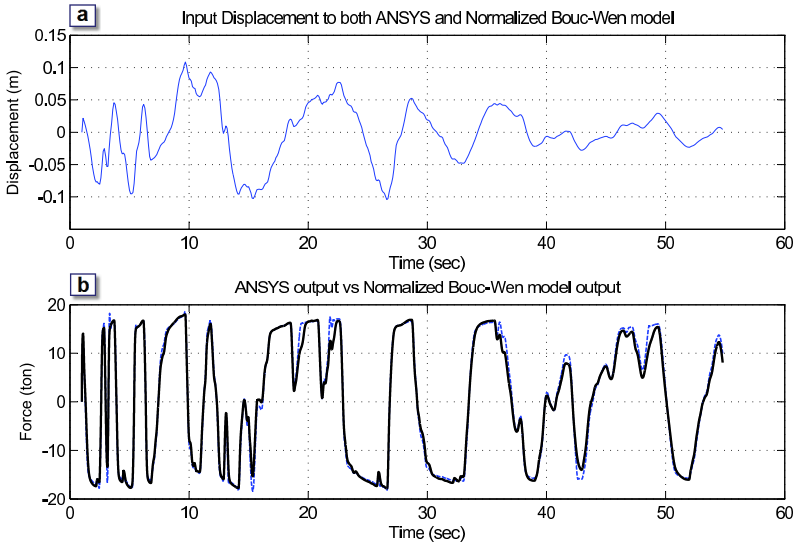

Figure 6.2: **(a)** Input displacement into ANSYS, and Bouc-Wen models; **(c)** ANSYS output vs Bouc-Wen model output, relative error $\varepsilon_1 = 5.70\%$ and $\varepsilon_\infty = 3.15\%$, respectively. ANSYS output (- - -), Models output (——) .

6.5 Implementation

An idealized single bay 5DOFs (including the suspended base) base-isolated concrete moment-resisting frame is considered in the present study as the example structure. It is modeled as a shear type structure mounted on the proposed isolation bearing, Fig. 6.3, with one lateral degree-of-freedom DOF at each floor. All the vibrational modes are included in the analysis. The assumptions given in Section 5.5 are also valid for the structural system under consideration in this chapter.

The cross sectional dimensions of the frame columns and beams are 0.70 $\times$ 0.25 m and 0.70 $\times$ 0.25 m, respectively. All the stories are 3.0 m height and the frame span is 5.0 m. The frame material is normal-weight concrete with a total material volume per frame of 8.60 m^3. This concrete material has the following isotropic properties:

- Weight per unit volume = 23563.12 N m^{-3}
- Mass per unit volume = 2402.77 Kg m^{-3}
- Modulus of elasticity = 2.486E+10 N m^{-2}
- Poisson's ratio = 0.20
- Shear modulus = 1.036E+10 N m^{-2}
- Specified concrete compressive strength = 27579032 N m^{-2}

The superstructure is idealized as a linear flexible building. The modal frequencies, periods, and the modal mass participation factor of the designed structure are listed in Table 6.2 where the damping ratio for all modes is kept fixed to 2% of the critical damping. The whole weight of the example frame structure (including the isolation bearings) is 1180 kN.

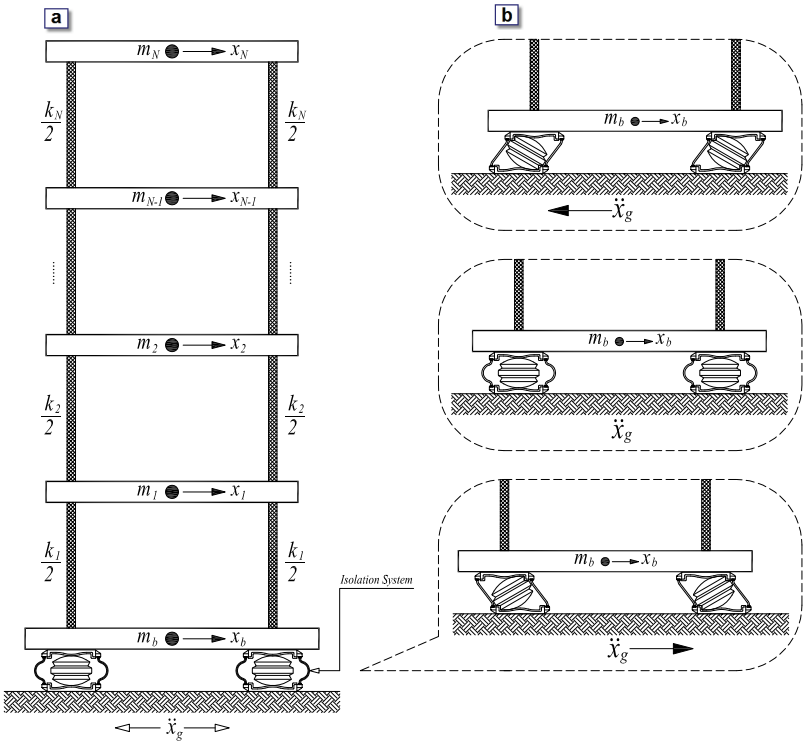

Figure 6.3: Case study structure.

6.5.1 Equations of motion

The equations of motion of an N-story linear shear type superstructure subjected to earthquake excitation is written in the matrix form

$$\mathbf{M}_\mathrm{s}\ddot{\mathbf{x}}_\mathrm{s} + \mathbf{C}_\mathrm{s}\dot{\mathbf{x}}_\mathrm{s} + \mathbf{K}_\mathrm{s}\mathbf{x}_\mathrm{s} = -\mathbf{M}_\mathrm{s}\{\mathbf{1}\}(\ddot{x}_\mathrm{b} + \ddot{x}_\mathrm{g}), \tag{6.1}$$

	Mode Number				
	Isolator	1	2	3	4
Fixed-base Structure					
Frequency (Hz)		4.674	13.335	20.066	24.072
Period (Sec)		0.214	0.075	0.050	0.042
Effective Modal Mass (%)		0.898	0.081	0.018	0.003
Base-isolated Structure					
Frequency (Hz)	0.341	7.815	15.023	20.744	24.217
Period (Sec)	2.932	0.128	0.067	0.048	0.041
Effective Modal Mass (%)	0.999	0.001	0.000	0.000	0.000

Table 6.2: Modal properties of fixed-base and isolated example structures.

where $\mathbf{M}_\mathrm{s}$, $\mathbf{K}_\mathrm{s}$, and $\mathbf{C}_\mathrm{s}$ are the $N \times N$ mass, stiffness and damping matrices of the superstructure, respectively; $\mathbf{x}_\mathrm{s} = \{x_1, x_2, \ldots, x_N\}^T$ is the relative displacement vector of the superstructure; $\dot{\mathbf{x}}_\mathrm{s}$ and $\ddot{\mathbf{x}}_\mathrm{s}$ are the relative velocity and acceleration vectors, respectively; $x_j (j = 1, 2, \ldots, N)$ is the lateral displacement of the jth floor relative to the base mass; $\{\mathbf{1}\} = \{1, 1, 1, \ldots, 1\}^T$ is the influence coefficient vector; $\ddot{x}_\mathrm{b}$ is the relative acceleration of the base mass; and $\ddot{x}_\mathrm{g}$ is the earthquake ground acceleration.

The governing equation of motion for the base mass is given by

$$m_\mathrm{b}\ddot{x}_\mathrm{b} + \eta F_\mathrm{b} - c_1\dot{x}_1 - k_1 x_1 = -m_\mathrm{b}\ddot{x}_\mathrm{g}, \tag{6.2}$$

where m_b is the mass of the base raft; c_1 and k_1 are the damping and stiffness of the first story, respectively; η is the total number of isolators and F_b is the restoring force transmitted to the base mass by a single RNC isolator. This force is expressed using the normalized Bouc-Wen model as

$$F_\mathrm{b}(t) = \kappa_x\, x_\mathrm{b}(t) + \kappa_w\, w(t), \tag{6.3}$$

$$\dot{w} = \rho(\dot{x}_\mathrm{b} - \sigma|\dot{x}_\mathrm{b}||w|^{n-1}w - (\sigma - 1)\dot{x}_\mathrm{b}|w|^n), \tag{6.4}$$

where κ_x, κ_w, ρ, σ and n are the shape controlling parameters of the hysteresis loop; $w(t)$ is an auxiliary variable which is not accessible to measurement and *dotw* denotes the time derivative. The lower value of the parameter σ is limited to $\frac{1}{2}$ and to guarantee BIBO stability, passivity, and consistency with physical asymptotic motion [200, 201].

6.5.2 Performance measures

The response quantities of interest are the top floor absolute acceleration, building drift, base shear and the relative-to-ground base displacement. These response quantities are of importance because floor accelerations developed in the superstructure are a measure of human comfort and are the main source

of damaging housed sensitive equipment. The building drift is the main cause of structural and nonstructural damage. The base shear and base moment govern the cross sectional dimensions of the lateral force supporting systems in structures, while the bearing (base) displacements are crucial in the design of isolation systems.

6.5.3 Simulation tool

Having the input data given in Section 6.5 and the assumptions given in Section 5.5, the case study structure shown in Fig. 6.3 is modeled using the Structural Analysis Program SAP2000 *advanced* [6]. The proposed RNC isolator is modeled as a nonlinear support, whose dynamic behavior is governed by the hysteretic Bouc-Wen model, (6.3)–(6.4), where the rest of the structure is assumed to behave linearly. The parameters of the Bouc-Wen model have been identified, in Section 6.4.1. The mechanical characteristics of the RNC–c isolator are obtained in Section 6.3 and incorporated into the simulation code along with the isolator mass. Then the structural mass, stiffness and damping matrices are formed and related to other variables as shown explicitly by Eqs. (6.1)–(6.2). A modal analysis is performed first to determine the dynamic properties, of the modeled system, that are listed in Table 6.2. Then, a linear and nonlinear dynamic analysis are carried out in cases of fixed-base and isolated base structures, respectively, under a variety of ground motion excitations to determine the response quantities given in Section 6.5.2.

6.5.4 Numerical study

In the following numerical study, extensive investigation of the RNC isolator is performed to assess its effectiveness. In Section 6.6, the behavior of the RNC isolator is investigated under fixed-amplitude variable-frequency harmonic ground motions, using frequency response analysis, considering different RNC characteristics. In Section 6.7, the behavior of the RNC isolator is investigated under strong earthquake ground motion, using time history analysis and considering different RNC characteristics. The influence of the superstructural flexibility is studied in Section 6.8. Finally, the influence of different earthquake characteristics including long period earthquakes is examined in Section 6.9.

6.6 Frequency response analysis

A frequency response analysis is conducted on the case study structure, Table 6.2, using fixed-amplitude variable-frequency harmonic ground motions, which is defined as a sinusoidal ground acceleration

$$\ddot{x}_{\mathrm{g}}(t) = 0.5g \sin(2\pi f_{\mathrm{g}} t) \tag{6.5}$$

where f_g denotes the excitation frequency and g is the gravitational acceleration. A wide frequency range of 0.05–2.0 Hz is considered. Both fixed-base and base isolated cases, using the three different RNC isolator design sets in Table 6.1, are investigated.

Fig. 6.4(a) shows the peak structural absolute accelerations as a function of the excitation frequency in Hz, using the three RNC–c isolator designs, in addition to the fixed-base acceleration that is included for comparison purpose. Fig. 6.4(b) shows the corresponding total building drift, expressed as the difference between topmost floor displacement and the base displacement, against the excitation frequency.

By comparing different curves in Fig. 6.4(a), one observes that except for very low excitation frequencies, which are unlikely to occur, the structural absolute acceleration is significantly reduced. This response reduction grows as we move from the stiffer design (RNC–c set I) toward the more flexible one (RNC–c set III). A single resonant peak is observed for each curve. Such peaks are shifted towards lower frequencies for softer RNC isolator designs. The Set I starts to be effective in reducing accelerations from 0.71 Hz up, while Sets II and III are efficient at lower frequencies of 0.46 Hz and 0.32 Hz, respectively. The same observations are almost the same regarding Fig. 6.4(b) except that the isolator Set I reduces building drift from a lower frequency of 0.58 Hz up.

6.7 Time history analysis

This section investigates the dynamic response of the isolated structure over the full time history of excitation. The strong-motion Kobe earthquake, of peak ground acceleration PGA = $0.68g$, is considered. Fig. 6.5(a,b,c) shows the absolute acceleration time history responses at the top floor considering the three RNC design sets I, II and III, respectively. From Fig. 6.5 it is obvious that the RNC isolator can significantly reduce the structural absolute accelerations under such strong-motion earthquake for all RNC sets along the excitation duration. The response reduction becomes more significant as the isolator flexibility increases Figs. 6.5(b,c) as the peak acceleration responses are $0.46g$, $0.32g$ and $0.21g$ for sets I, II and III, respectively, where it was $2.93g$ in the case of fixed-base structure. The recorded associated base displacement for all cases is always below 0.38 m, which is reasonable and can be accommodated by the RNC isolator without affecting its stability nor reducing its load carrying capacity.

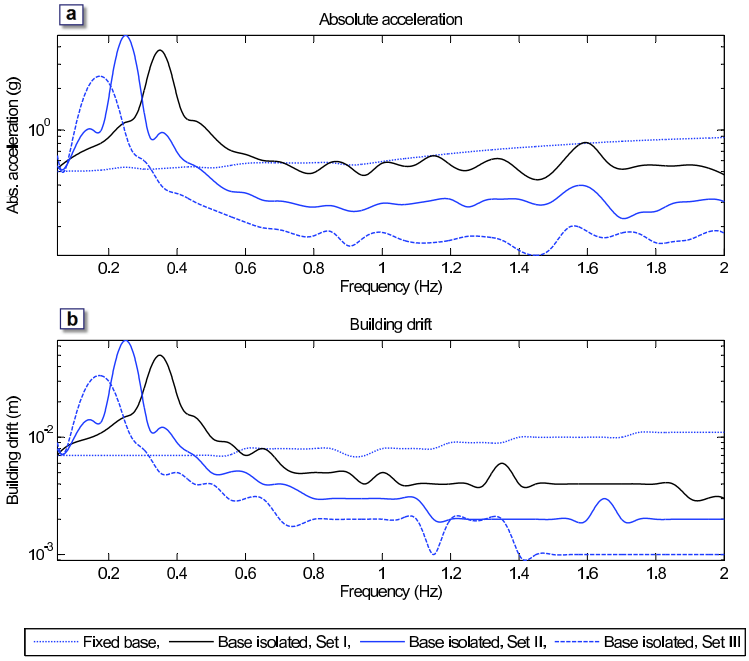

Figure 6.4: Frequency response of different designs of RNC–c isolator: (a) Absolute acceleration at the topmost floor, (b) Whole building drift.

6.8 Influence of superstructure flexibility

The flexibility in the base-isolated structure is mainly concentrated at the isolation level. As a result, the response of the base-isolated structure can be investigated by modeling the superstructure as rigid [508, 86, 224]. However, it will be interesting to compare the seismic response of a RNC-base-isolated structure in two cases with the superstructure modeled as rigid and flexible, respectively, to study the influence of the superstructure flexibility. The isolation systems are robust and practically useful when they are effective for different structures with wide range of properties. For dynamic response, the most important property is the fundamental time period of the structure. For most typical building structures, the fundamental time period varies between 0.1 to $0.50sec$. Tall buildings and flexible structures such as bridges have periods of up to $2sec$ or longer. Base isolator derives its effectiveness by increasing the time period of the structure. It is therefore essential that the fundamental period of the structure be shorter than the period of the isolator. However, the most suitable structures for seismic isolation are those with short natural period, less than about $1sec$. This is the case for concrete buildings less than 10 stories and for flexible types of structures, such as steel moment frames, less

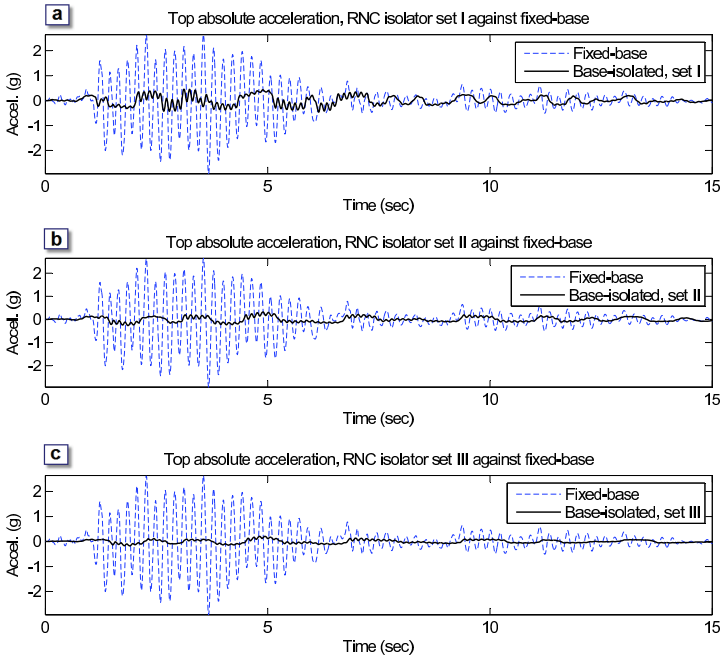

Figure 6.5: Acceleration time histories under Kobe earthquake using different RNC isolator sets: (a) Set I, (b) Set II, (c) Set III.

than 5 stories. In this investigation, the time period of the RNC isolator, T_{b}, is chosen as $4.15sec$ (set II, as the average design set), and a reasonable wide range of structural time period from 0.10 to $1.20sec$ has been considered along with a perfectly rigid structure. These choices correspond to the most likely practical values of these parameters. The response quantities of interest are absolute acceleration of the structure and bearing displacement.

Table 6.3 shows the variations of top floor absolute acceleration and bearing displacement of a 5DOFs RNC-base-isolated structure against the superstructure fundamental time period, T_{s}, under three different ground acceleration records having low (Kern of PGA=$0.179g$), moderate (El Centro of PGA=$0.348g$), and high intensity (Northridge of PGA=$0.883g$). As expected, the isolation bearing performs well as the structural period is lower than 1 sec for all the three earthquakes. However, under low intensity Kern earthquake, as structural flexibility continues to increase, the isolation tends to be a burden. This is not the case under moderate (El Centro) and high intensity (Northridge) earthquakes where the proposed isolator is still effective up to

1.20 sec period. Practically, if the structure has a long period, then no much benefit from isolation is expected, although in some cases, energy dissipation at the base may help. This is used quite often in bridges with a long period, but not so often for buildings.

Further inspection of Table 6.3 shows a substantial increase in the top floor acceleration as the fundamental time period of the isolated superstructure increases. This implies that the superstructure accelerations will be underestimated if the superstructure flexibility is ignored and it is modeled as a rigid body. The increase in the superstructure accelerations is found to be more pronounced for high PGA excitation. On the other hand, the bearing displacement is not much influenced with the increase in the superstructure flexibility. Thus, the flexibility of superstructure increases the superstructure acceleration but it does not have significant influence on the bearing displacements. Moreover, the efficiency of the proposed RNC isolator is almost independent of the structural time period, especially as the excitation intensity increases.

6.9 Influence of isolator properties and earthquake characteristics

This section is devoted to investigate the robustness of the RNC isolator under different earthquake characteristics. For relatively general results, the three design sets as well as a wide range of structural fundamental periods are considered. This investigation is carried out following three steps:

- In the first step, the three design sets of the RNC and a wide range of structural fundamental periods of 0.00 sec– 1.20 sec are considered. Three scaled intensities (PGA = 50%, 100% and 200%) of El Centro earthquake are used, in order to investigate the influence of earthquake amplitude on the RNC behavior. The chosen performance measures are the top floor absolute acceleration and base displacement. The results of this step are listed in Tables 6.4–6.6.

- In the second step, the influence of the long-period earthquakes on the RNC-isolated structure behavior is investigated. The 1985 long-period Mexico City earthquake is used along with the same range fundamental periods range of the first step. Only the RNC set II is considered for a single case study structure having a fundamental period of 0.215 sec. The performance measures are chosen as the base displacement, base shear, top absolute acceleration and whole building drift, which is expressed as the difference between the top floor and the base mass displacements. The results are shown in Fig. 6.6.

- In the third step, the robustness of the RNC isolator under a wide range of excitations is checked. Only the RNC set II is considered for a single case study structure having a fundamental period of 0.215 sec. A set of 36 earthquakes is used to excite the structure. The performance measures are the same as in the second step. The results are listed in Table 6.7.

From Tables 6.4-6.6, the following conclusions can be drawn from the first step:

1. The RNC isolator efficiency in reducing structural accelerations is higher under higher intensity excitations, and it is more significant at the time period that corresponds to the maximum fixed-base response.
2. Higher intensity excitation widens the period range on which the RNC isolator can mitigate the structural response efficiently.
3. As the excitation intensity is doubled, the fixed-base response is exactly doubled but the fixed-base response is not.
4. With the decrease in the isolator elastic stiffness, k_e (moving from set I to set III), the top floor absolute acceleration decreases substantially. On the other hand, the bearing displacement shows marginal increasing trend with the decrease in the isolator elastic stiffness, but decreases with the increase of structural flexibility under the same excitation. This implies that the elastic stiffness of the isolator has significant effects on the response of the base-isolated structure.
5. With the increase in the isolator characteristic strength Q (the intersection of hysteresis loop with vertical y axis) the top floor acceleration increases and the bearing displacement decreases. This is expected, because for higher isolator characteristic strengths, the isolation system remains much longer time in the elastic state, which produces less flexibility in the structural system and thereby less energy dissipation. As a result, the superstructure acceleration increases and the bearing displacement decreases with the increase of the isolator characteristic strength. Thus, it can be concluded that the response of the base-isolated structure is significantly influenced by the characteristic strength of the isolator.

Fig. 6.6 displays the four response quantities of interest under the long-period Mexico City earthquake. From this figure, the following observations can be made:

1. The bearing displacements are relatively small and can be simply accommodated by the RNC isolator.
2. The RNC isolator reduces the building drift for all structural periods, specially at long structural periods.
3. The RNC is reasonably effective in reducing the acceleration response at short periods (up to 0.70 sec).
4. Considering the base shear, the RNC exhibits a relatively robust behavior for all the considered structural periods.

Therefore, the RNC isolator is a reasonably useful isolation device for a reasonable range of fundamental structural periods under long-period earthquakes.

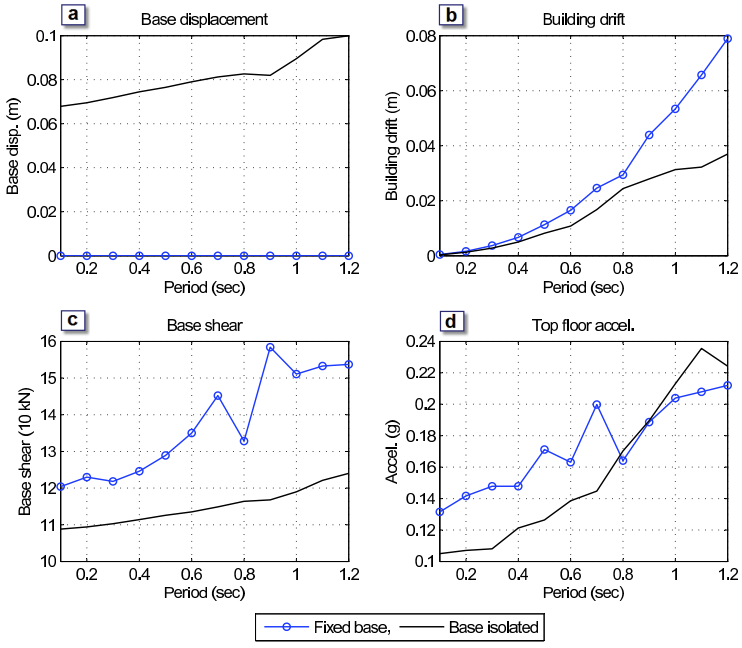

Figure 6.6: Response spectra of RNC-isolated structure under long-period Mexico City earthquake: (a) Base displacement, (b) Building drift, (c) Base shear, (d) Top floor absolute acceleration.

Table 6.7 presents the results of the extensive study under a wide set of distinct earthquake ground motions (third step) using the RNC isolator set II. The same response quantities of interest used in the second step are used as performance measures. The main observation from this table is the great ability of the proposed RNC isolator to reduce all the four response quantities under consideration regardless the amplitude and frequency content of the ground motion excitation.

In summary, the analysis performed in this section shows that the RNC isolator may be seen as a robust isolation device under variations in earthquake characteristics including long-period earthquakes, since its efficiency is almost independent of both the amplitude and frequency content of excitation thereby preserving the most significant advantage of ideal isolation system.

6.10 Conclusions

Chapters 3 and 4 presented a detailed description of the main principles of operation, modeling and characterization of the RNC–c isolator. This isolator is intended to protect light- to moderate mass systems from seismic hazards, for which their lower mass has to be associated with lower isolator stiffness to achieve effective isolation. In this chapter, an extensive numerical evaluation of the performance of such RNC isolator has been presented. The numerical investigations affirmed the effectiveness of the device by attaining significant reduction of the light- to moderate building accelerations, drifts and base shears, while keeping reasonable base displacement. Even when very flexible structures are isolated and long time-period excitations are considered, the proposed system is found to be highly effective. Further, the proposed RNC isolation bearing is found to exhibit a robust performance for a wide range of structures, isolators and ground motion characteristics. This concludes that the RNC–c isolator can be seen as a successful isolation device for light- to moderate building structures. ■

T_s (sec)	KERN Earthquake			EL-CENTRO Earthquake			NORTHRIDGE Earthquake		
	Isolated Structure		Fixed-base S.	Isolated Structure		Fixed-base S.	Isolated Structure		Fixed-base S.
	$\ddot{x}_{\text{top}}$ (m/sec^2)	x_{base} (m)	$\ddot{x}_{\text{top}}$ (m/sec^2)	$\ddot{x}_{\text{top}}$ (m/sec^2)	x_{base} (m)	$\ddot{x}_{\text{top}}$ (m/sec^2)	$\ddot{x}_{\text{top}}$ (m/sec^2)	x_{base} (m)	$\ddot{x}_{\text{top}}$ (m/sec^2)
0.0	1.05	0.032	1.76	1.13	0.066	3.41	1.22	0.096	8.66
0.1	1.05	0.032	2.48	1.18	0.066	9.74	1.22	0.096	21.53
0.2	1.21	0.033	7.60	1.62	0.067	11.23	2.24	0.097	39.79
0.3	1.68	0.035	6.94	2.03	0.067	10.21	3.61	0.099	21.26
0.4	1.88	0.032	6.43	3.81	0.074	10.19	5.53	0.106	17.42
0.5	2.41	0.031	5.06	3.48	0.059	13.28	5.40	0.107	12.56
0.6	2.79	0.028	5.65	3.69	0.069	10.66	4.54	0.093	13.70
0.7	2.67	0.022	3.89	3.45	0.066	10.37	5.25	0.097	16.91
0.8	2.69	0.018	3.88	4.26	0.058	8.46	5.09	0.097	17.34
0.9	3.10	0.017	4.55	4.09	0.045	8.61	5.73	0.083	13.16
1.0	3.40	0.021	3.11	4.23	0.052	6.32	6.81	0.084	11.34
1.1	3.70	0.019	3.00	4.45	0.060	6.05	6.24	0.067	9.99
1.2	3.59	0.017	3.19	4.06	0.054	5.32	5.83	0.076	7.23

Table 6.3: Effect of superstructure flexibility, isolation set II.

T_s (sec)	EL-CENTRO (50% PGA)			EL-CENTRO (100% PGA)			EL-CENTRO (200% PGA)		
	Isolated Structure		Fixed-base S.	Isolated Structure		Fixed-base S.	Isolated Structure		Fixed-base S.
	$\ddot{x}_{\text{top}}$ (m/sec^2)	x_{base} (m)	$\ddot{x}_{\text{top}}$ (m/sec^2)	$\ddot{x}_{\text{top}}$ (m/sec^2)	x_{base} (m)	$\ddot{x}_{\text{top}}$ (m/sec^2)	$\ddot{x}_{\text{top}}$ (m/sec^2)	x_{base} (m)	$\ddot{x}_{\text{top}}$ (m/sec^2)
0.00	1.92	0.026	1.71	2.07	0.042	3.41	2.35	0.110	6.82
0.10	1.97	0.026	4.87	2.23	0.042	9.74	2.77	0.110	19.48
0.20	2.45	0.023	5.61	2.97	0.044	11.22	3.99	0.107	22.44
0.30	2.70	0.025	5.11	4.68	0.042	10.22	6.02	0.107	20.44
0.40	3.83	0.025	5.10	6.62	0.045	10.20	10.04	0.130	20.40
0.50	4.46	0.021	6.64	7.52	0.053	13.28	9.90	0.093	26.56
0.60	4.17	0.022	5.33	6.51	0.051	10.66	8.10	0.088	21.32
0.70	4.22	0.018	5.19	7.00	0.037	10.38	9.24	0.092	20.76
0.80	4.26	0.016	4.23	6.60	0.044	8.46	9.15	0.090	16.92
0.90	3.62	0.017	4.31	6.53	0.034	8.62	9.26	0.088	17.24
1.00	3.58	0.011	3.16	6.21	0.026	6.32	10.10	0.079	12.64
1.10	3.30	0.010	3.02	5.70	0.025	6.04	9.02	0.090	12.08
1.20	2.96	0.008	2.66	5.68	0.021	5.32	9.51	0.091	10.64

Table 6.4: Effects of isolator properties and earthquake intensity, utilizing the isolation set I.

T_s (sec)	EL-CENTRO (50% PGA)			EL-CENTRO (100% PGA)			EL-CENTRO (200% PGA)		
	Isolated Structure		Fixed-base S.	Isolated Structure		Fixed-base S.	Isolated Structure		Fixed-base S.
	$\ddot{x}_{\text{top}}$ (m/sec^2)	x_{base} (m)	$\ddot{x}_{\text{top}}$ (m/sec^2)	$\ddot{x}_{\text{top}}$ (m/sec^2)	x_{base} (m)	$\ddot{x}_{\text{top}}$ (m/sec^2)	$\ddot{x}_{\text{top}}$ (m/sec^2)	x_{base} (m)	$\ddot{x}_{\text{top}}$ (m/sec^2)
0.00	0.98	0.035	1.71	1.13	0.066	3.41	1.45	0.141	6.82
0.10	0.98	0.035	4.87	1.18	0.066	9.74	1.54	0.141	19.48
0.20	1.22	0.033	5.61	1.62	0.067	11.22	2.08	0.141	22.44
0.30	1.59	0.032	5.11	2.03	0.067	10.22	3.82	0.142	20.44
0.40	2.17	0.030	5.10	3.81	0.074	10.20	5.67	0.157	20.40
0.50	2.29	0.027	6.64	3.47	0.059	13.28	5.00	0.139	26.56
0.60	2.60	0.029	5.33	3.69	0.069	10.66	4.66	0.140	21.32
0.70	2.44	0.029	5.19	3.45	0.066	10.38	5.91	0.138	20.76
0.80	2.42	0.024	4.23	4.26	0.058	8.46	6.53	0.149	16.92
0.90	2.53	0.019	4.31	4.08	0.045	8.62	5.80	0.149	17.24
1.00	2.48	0.019	3.16	4.23	0.052	6.32	7.19	0.157	12.64
1.10	2.44	0.019	3.02	4.45	0.060	6.04	6.89	0.140	12.08
1.20	2.29	0.014	2.66	4.06	0.054	5.32	6.14	0.117	10.64

Table 6.5: Effects of isolator properties and earthquake intensity, utilizing the isolation set II.

T_s (sec)	EL-CENTRO (50% PGA)			EL-CENTRO (100% PGA)			EL-CENTRO (200% PGA)		
	Isolated Structure		Fixed-base S.	Isolated Structure		Fixed-base S.	Isolated Structure		Fixed-base S.
	$\ddot{x}_{\text{top}}$ (m/sec^2)	x_{base} (m)	$\ddot{x}_{\text{top}}$ (m/sec^2)	$\ddot{x}_{\text{top}}$ (m/sec^2)	x_{base} (m)	$\ddot{x}_{\text{top}}$ (m/sec^2)	$\ddot{x}_{\text{top}}$ (m/sec^2)	x_{base} (m)	$\ddot{x}_{\text{top}}$ (m/sec^2)
0.00	0.55	0.047	1.71	0.71	0.091	3.41	1.04	0.153	6.82
0.10	0.55	0.047	4.87	0.71	0.091	9.74	1.18	0.153	19.48
0.20	0.60	0.047	5.61	0.80	0.092	11.22	1.66	0.153	22.44
0.30	0.65	0.047	5.11	1.03	0.092	10.22	1.79	0.153	20.44
0.40	1.02	0.046	5.10	2.04	0.093	10.20	3.08	0.153	20.40
0.50	1.12	0.044	6.64	1.76	0.094	13.28	2.27	0.152	26.56
0.60	1.23	0.045	5.33	1.19	0.092	10.66	2.82	0.154	21.32
0.70	1.29	0.045	5.19	2.50	0.089	10.38	3.11	0.153	20.76
0.80	1.46	0.046	4.23	2.28	0.097	8.46	3.53	0.150	16.92
0.90	1.67	0.036	4.31	2.42	0.092	8.62	4.00	0.153	17.24
1.00	1.65	0.028	3.16	2.90	0.087	6.32	4.27	0.151	12.64
1.10	1.84	0.027	3.02	2.82	0.075	6.04	3.40	0.147	12.08
1.20	1.80	0.027	2.66	2.50	0.080	5.32	4.00	0.148	10.64

Table 6.6: Effects of isolator properties and earthquake intensity, utilizing the isolation set III.

No	Earthquake	PGA	x_b	Base Shear (ton)			Abs. Top Acceleration (g)			Building Drift (m)		
		(g)	(m)	Isolated	Fixed-base	%[a]	Isolated	Fixed-base	%	Isolated	Fixed-base	%
1	ALTADENA 0°	0.45	0.0455	13.88	91.33	85 %	1.93	13.48	86 %	0.0018	0.0155	88 %
2	ALTADENA 90°	0.18	0.0146	8.15	24.66	67 %	0.79	3.78	79 %	0.0011	0.0044	75 %
3	ARRAY06 0°	0.38	0.1712	15.22	81.85	81 %	1.60	11.67	86 %	0.0019	0.0146	87 %
4	ARRAY06 90°	0.44	0.3460	20.19	72.11	72 %	1.99	10.33	81 %	0.0025	0.0119	79 %
5	CORRALIT 0°	0.63	0.1011	19.53	125.98	85 %	2.51	17.25	85 %	0.0023	0.0209	89 %
6	CORRALIT 90°	0.48	0.1108	15.42	96.21	84 %	2.05	15.17	86 %	0.0019	0.0179	89 %
7	HOLLISTE 0°	0.37	0.2099	17.40	59.05	71 %	2.13	6.60	68 %	0.0023	0.0085	73 %
8	HOLLISTE 90°	0.18	0.0570	12.28	32.85	63 %	1.36	4.43	69 %	0.0016	0.0053	70 %
9	LACC NOR 0°	0.22	0.0489	12.68	37.17	66 %	1.25	5.72	78 %	0.0015	0.0067	78 %
10	LACC NOR 90°	0.26	0.0376	12.26	90.57	86 %	1.18	14.31	92 %	0.0014	0.0173	92 %
11	LEXINGT 0°	0.44	0.1665	18.69	70.46	73 %	2.01	9.30	78 %	0.0019	0.0115	84 %
12	LEXINGT 90°	0.41	0.1869	19.70	67.75	71 %	2.03	9.55	79 %	0.0021	0.0116	82 %
13	LUCERNE 0°	0.68	0.0641	13.46	61.90	78 %	1.34	20.65	94 %	0.0016	0.0101	84 %
14	LUCERNE 90°	0.70	0.0417	15.65	106.81	85 %	1.65	18.67	91 %	0.0017	0.0194	91 %
15	NEW HALL 0°	0.59	0.2466	21.76	175.66	88 %	2.90	25.02	88 %	0.0025	0.0302	92 %
16	NEW HALL 90°	0.58	0.1000	19.30	131.95	85 %	2.06	20.70	90 %	0.0020	0.0246	92 %
17	OAK WHAF 0°	0.29	0.0944	14.19	49.66	71 %	1.64	7.06	77 %	0.0018	0.0085	79 %
18	OAK WHAF 90°	0.27	0.1401	15.07	44.28	66 %	1.80	5.76	69 %	0.0019	0.0070	73 %
19	PETROLIA 0°	0.59	0.1160	17.16	107.12	84 %	2.65	16.47	84 %	0.0022	0.0196	89 %
20	PETROLIA 90°	0.66	0.3015	23.92	82.71	71 %	2.95	12.38	76 %	0.0029	0.0131	78 %
21	POMONA 0°	0.19	0.0201	10.32	66.08	84 %	1.00	9.58	90 %	0.0013	0.0118	89 %
22	POMONA 90°	0.21	0.0182	9.36	30.91	70 %	1.04	5.69	82 %	0.0013	0.0062	79 %
23	SANTA MONICA 0°	0.37	0.0449	12.32	85.63	86 %	1.65	13.58	88 %	0.0017	0.0160	89 %
24	SANTA MONICA 90°	0.88	0.0980	14.38	266.58	95 %	2.16	43.02	95 %	0.0021	0.0505	96 %
25	SYLMAR 0°	0.84	0.3001	27.00	124.98	78 %	2.55	15.73	84 %	0.0024	0.0186	87 %
26	SYLMAR 90°	0.60	0.1934	17.96	93.82	81 %	2.36	10.19	77 %	0.0023	0.0134	83 %
27	YERMO 0°	0.15	0.0499	11.46	45.44	75 %	1.10	6.48	83 %	0.0014	0.0078	82 %
28	YERMO 90°	0.24	0.1079	13.58	45.82	70 %	1.43	5.76	75 %	0.0017	0.0071	76 %
29	EL CENTRO	0.35	0.0678	13.54	61.83	78 %	1.77	9.85	82 %	0.0017	0.0114	85 %
30	KERN	0.18	0.0334	11.82	51.57	77 %	1.23	7.88	84 %	0.0014	0.0094	85 %
31	KOBE	0.68	0.3810	27.92	188.37	85 %	3.14	28.73	89 %	0.0030	0.0337	91 %
32	LOMA PRIETA	0.28	0.0874	14.82	58.75	75 %	1.83	8.01	77 %	0.0018	0.0098	82 %
33	MEXICO	0.10	0.0697	10.95	13.98	22 %	1.05	1.41	26 %	0.0014	0.0019	26 %
34	NORTHRIDGE	0.88	0.0980	14.38	266.58	95 %	2.16	43.02	95 %	0.0021	0.0505	96 %
35	PARKFIELD	0.24	0.0210	9.91	44.15	78 %	1.00	7.26	86 %	0.0013	0.0082	84 %
36	SAN FERNANDO	1.17	0.3239	24.44	291.55	92 %	3.28	47.62	93 %	0.0030	0.0556	95 %
				Average Reduction (%)		77 %	Average Reduction (%)		82 %	Average Reduction (%)		83 %

Table 6.7: Summary of isolated vs non-isolated responses using isolator set II, ton-m-sec units

[a]Reduction as a percentage of the corresponding fixed-base response

7 Equipment isolation: isolated raised floor approach

7.1 Introduction

Seismic isolation is presently established as the most effective way to mitigate the vibrational response of sensitive equipment housed in structures under earthquake attacks [187, 301]. This is particularly important in critical facilities as hospitals, emergency centers, communication and data centers as well as museums. In general, there are three approaches to isolate sensitive equipment [170]: (1) isolation of the entire housing structure, (2) isolation of a single equipment, and (3) isolation of raised floor systems. The first approach is most appropriate for new construction. Isolators are installed between the structure and its foundation with the objective of reducing the damage of both the primary structure and its contents [333]. The second approach appeared even before the application of seismic isolation in buildings. However, it is usually confronted with a number of problems including the extreme difficulty of achieving the desired long period while keeping affordable displacement and ensuring enough vertical stiffness to support the equipment itself [115, 270].

As for the third approach, the sensitive equipment is mounted on a secondary raised-floor, which is attempted to be decoupled from the building floor by means of isolation systems. This approach is valid for new construction and retrofitting as well. It has the potential of offering the best of the first approach with lower cost while avoiding the main drawbacks of the second one. Therefore, isolated raised floor systems are now well established as an effective technique for mitigation of the seismic risk posed on equipment. This is the approach considered in this chapter.

A variety of passive, active, semi-active and hybrid isolation systems has been proposed in the literature. Commonly, equipment passive isolation systems are of a sliding-based or rolling-based type [237, 332]. Flat sliding bearings are the simplest form of sliding-based devices, but they lack buffer and efficient re-centering mechanisms. They were used for equipment isolation in [302]. These drawbacks were overcome in [12] through spherically shaped sliding plates in a so called friction pendulum system (FPS) but on account of equipment uplift. In [270], comprehensive shake table tests were performed on FPS-isolated raised floor systems used in computer centers. However, FPS tend not to be cost effective for light mass systems. Indeed, regardless of the vertical weight, the displacement is the same for a given effective period and so the size of the slide plates, which are the most expensive part of sliding bearings, is the same for heavy or light mass systems. Another sliding approach, named sliding concave foundation (SCF) system, was presented in [171] and investigated analytically in [170] when used as the isolation device for raised-floor systems. However, it may cause permanent tilting of the isolated object.

Rolling-based bearings offer the maximum equipment-base horizontal decoupling, but they lack damping, buffer and re-centering mechanisms [291, 290, 222]. Reference [225] benefited from the elliptical shape of rollers to ensure a gravity-based re-centering mechanism. However, this shape causes equipment uplift and can not prevent permanent equipment dislocation under strong earthquakes. To overcome this difficulty, spherical rollers inside two opposite concave plates are proposed in [517] as a rolling-pendulum system. This provides a gravity restoring force without permanent displacement but damping is still missing, uplift is exhibited and the system has a fixed vibration period.

Sliding-pendulum and rolling-pendulum systems provide a natural period of 2–4 sec [155]. This period range is not sufficient for effective isolation of light mass systems, as low masses must be associated with low stiffness to achieve the required isolation period [248, 115, 270]. Moreover, based on their principle of operation, these systems force the isolated object to oscillate as a simple pendulum with a fixed vibration period, which represents a severe practical difficulty of aseismic design. In other words, these isolation systems employ a relatively fixed geometry, which makes the isolator not suitable for a wide range of structure and ground motion characteristics [331]. Some recent studies tried to enhance the adaptability of FPS [331, 145, 144].

Alternatively to passive isolation systems, [470, 468, 469, 489] explored the possibility of using a hybrid platform to protect equipment from seismic damage. In [142, 155, 15], the performance and reliability of semi-active equipment isolation was examined. A smart isolation system that combines an isolation platform with a variable friction device is proposed in [301]. This class of systems are appealing and have a good potential for isolation, but they require sensors and actuators with feedback control loops, which make them more complex than purely passive systems. While research on smart controlled systems

is developing, passive isolation systems may be still improvable to offer higher performance keeping design and implementation simplicity in comparison with active or semi-active systems.

In this chapter, a reduced-scale of the RNC–c isolator is selected for sensitive equipment protection, using the raised floor approach. The effectiveness of the RNC–c isolator is numerically assessed considering the case of equipment housed in upper floors of a building, where the accelerations are amplified and the motion contains strong components at long periods. Such case studies are presented in Section 7.5 and the corresponding results are given in Section 7.6.

7.2 The used RNC isolator type

In this chapter, a reduced scale RNC–c isolator that is more suitable for light-mass systems, is designed to suit the isolation of a secondary raised floor system, on which the motion sensitive equipment are mounted, while the housing structure is fixed-based. The RNC–c isolator type is shown in Fig. 3.1. For the designed reduced scale RNC–c isolator, the horizontal and vertical distances between the furthermost points are 0.496 m and 0.28 m, respectively.

7.3 Mechanical characteristics

Following the mechanical characterization scheme described in Section 4.2, the designed reduced scale RNC–c isolator used in this chapter has the following mechanical characteristics:

- Maximum vertical load capacity = 60 kN.
- Pre-yield stiffness = 30 kN m^{-1}
- Post-yield stiffness = 0.229 kN m^{-1}
- Yield displacement = 2.70 mm
- Yield force = 0.084 kN

7.4 Hysteretic modeling

The characterization described in Chapter 4 has shown that the reduced scale RNC–c isolator exhibits a hysteretic behavior, as shown in Fig. 7.1. The objective of this section is to obtain an input-output mathematical model to describe in a reasonable and manageable form the force-displacement relationship exhibited by the RNC–c isolator using the Bouc-Wen model of smooth hysteresis, described in Section 4.5. The normalized form of the Bouc-Wen model is used in this chapter. Such form of the model is defined in Section 4.5.4.

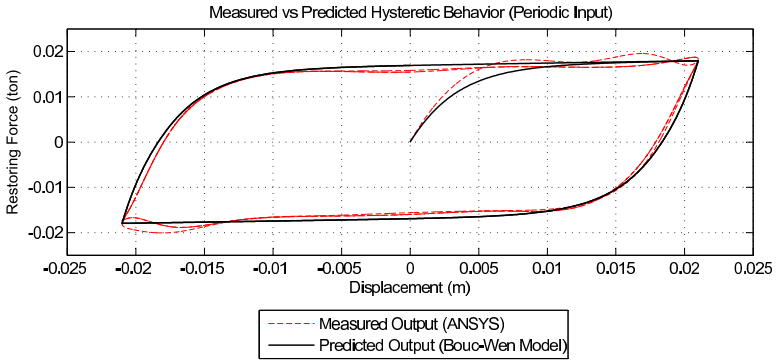

Figure 7.1: Measured vs calculated restoring force, under sinusoidal excitation, for 20% shear strain.

7.4.1 Bouc-Wen model parameters estimation

The normalized Bouc-Wen form provides an exact and explicit expression for the hysteretic limit cycle [200, 199]. Moreover, by using a periodic input signal $x(t)$ along with the analytic description of the limit cycle, a robust parametric nonlinear, nonrecursive identification method was presented in [201, 194]. This method is used in this chapter. For identification, the ANSYS code characterization described in Section 4.2 is used as the "true" isolator device. A periodic input horizontal displacement $x(t)$ is applied at the lowermost surface and the "measured" force is obtained at the topmost surface of the RNC isolator.

The values of the identified parameters of the normalized Bouc-Wen are:

$$\kappa_{\mathrm{x}} = 0.047; \quad \kappa_{\mathrm{w}} = 0.0155; \quad \rho = 307.68; \quad \sigma = 0.95; \quad n = 1.12$$

These values guarantee that the model is consistent with basic physical properties as bounded-input bounded-output stability and energy dissipation [199].

In Fig. 7.1, the measured output restoring force of the isolator is plotted against the calculated one via the identified normalized Bouc-Wen model. The good matching supports the accuracy of the Bouc-Wen model to capture the nonlinear hysteretic behavior of the RNC isolator.

7.4.2 Seismic verification of the Bouc-Wen model

To check the validity of the identified parameters, an actual random seismic displacement (half-scaled-amplitude Parkfield Earthquake) is used as an input for the Bouc-Wen model and the true system. The discrepancy between the measured and predicted outputs, F_{m} and F_{b}, is quantified using the L_1 and

L_∞-norms and the corresponding relative errors ε:

$$||f||_1 = \int_0^{T_e} |f(t)|\,\mathrm{d}\,t\,; \quad ||f||_\infty = \max_{t\in[0,T_e]} |f(t)|\,; \quad \varepsilon_{1,\infty} = \frac{||F_\mathrm{m} - F_\mathrm{b}||_{1,\infty}}{||F_\mathrm{m}||_{1,\infty}} \tag{7.1}$$

The relative error ε_1 quantifies the ratio of the bounded area between the output curves to the area of the measured force along the excitation duration T_e, while ε_∞ measures the relative deviation of the peak force.

Fig. 7.2 shows the close matching of both measured and predicted output curves with a relatively small error. Hence, the Bouc-Wen model can be considered a good practical mathematical description of the proposed RNC isolator for further analysis.

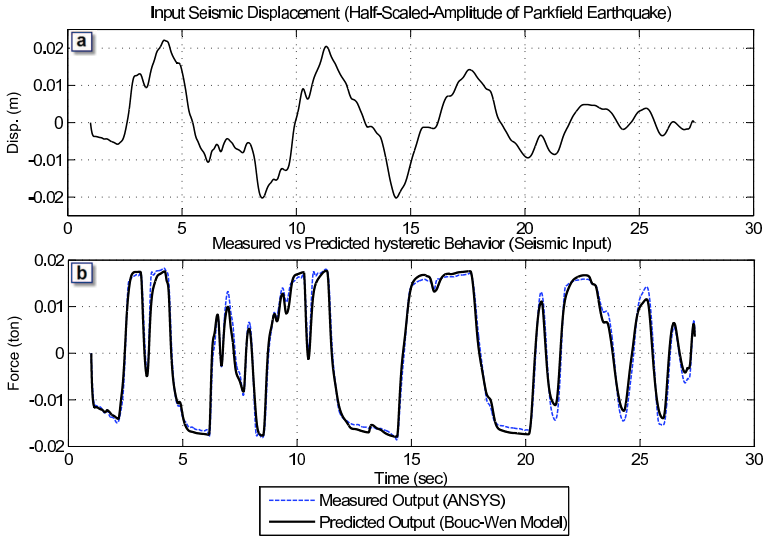

Figure 7.2: (a) Half-scaled-amplitude of Parkfield earthquake that is used as input seismic displacement, (b) Measured vs calculated restoring force for seismic input (Parkfield), the relative errors are $\varepsilon_1 = 4.4\%$ and $\varepsilon_\infty = 3.7\%$.

7.5 Implementation

In this section, we consider the case of equipment mounted on a raised-floor. The raised-floor is connected to the 7th floor of a primary eight storey structure (Fig. 7.3) through RNC isolators to examine their ability to mitigate the response of equipment housed in upper floors where the seismic acceleration is significantly amplified and the motion contains strong components at long periods. In this implementation, four RNC isolators are used to support the

secondary raised floor, one at each corner. Such isolators have the mechanical characteristics defined in Section 7.3.

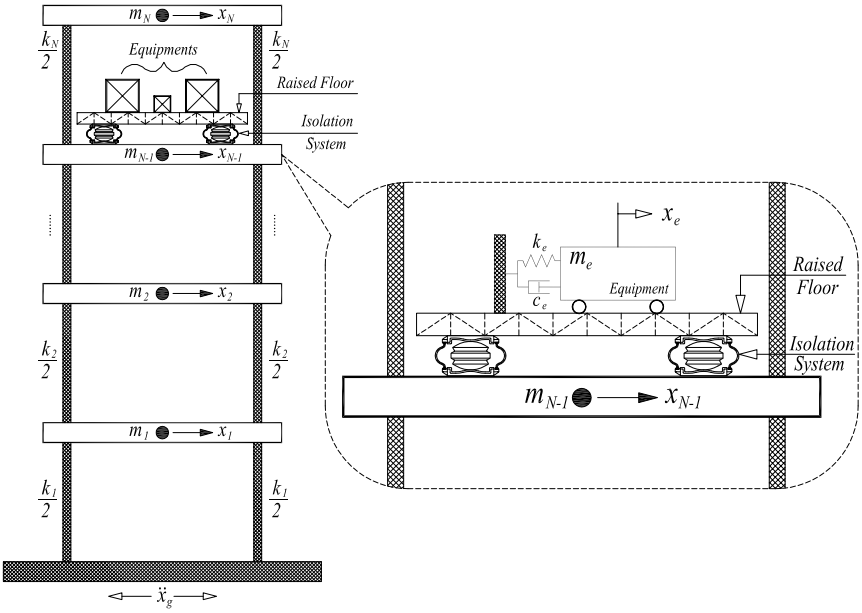

Figure 7.3: Idealized building, raised-floor and equipment model.

For comparison purposes, three cases are studied as illustrated in Fig. 7.4: (a) the isolated raised-floor is installed in a fixed base structure, *case I*; (b) non-isolated equipment is housed in a structure isolated by RNC isolators scaled to support the whole housing structure, *case II*; (c) non-isolated equipment is housed in a fixed-base structure, *case III*. In all cases, the structure has the same characteristics.

The supporting structure is a reinforced concrete moment resisting frame modeled as a shear building, where all significant vibrational modes, the structure-equipment-interaction, and the isolator nonlinearities are included in the performed analysis in order to get more realistic results. The assumptions given in Section 5.5 are also valid for the structural system under consideration in this chapter. The cross sectional dimensions of the frame columns and beams are 1.0×0.25 m and 0.70×0.25 m, respectively. All the stories are 3.0 m height and the frame span is 5.0 m. The frame material is normal-weight concrete with a total material volume per frame of 19 m^3. This concrete material has the following isotropic properties:

- Weight per unit volume = 23563.12 N m^{-3}
- Mass per unit volume = 2402.77 Kg m^{-3}

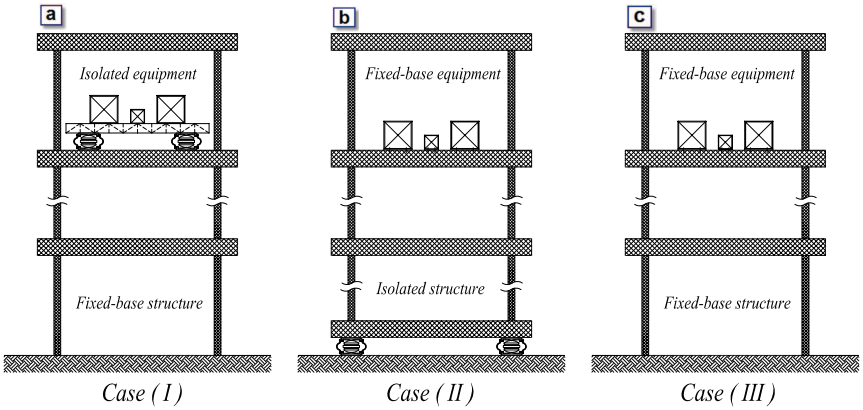

Figure 7.4: (a) The case of isolated raised-floor housed in a fixed-base structure, (b) The case of fixed-base equipment housed in an isolated-base structure, (c) The case of fixed-base equipment housed in a fixed-base structure.

- Modulus of elasticity = 2.486E+10 N m^{-2}
- Poisson's ratio = 0.20
- Shear modulus = 1.036E+10 N m^{-2}
- Specified concrete compressive strength = 27579032 N m^{-2}

Three example structures are considered having lateral stiffness matrices $\frac{1}{2}\mathbf{K}_\mathrm{s}$, $\mathbf{K}_\mathrm{s}$ and $2\mathbf{K}_\mathrm{s}$. The structural damping ratio for all modes is fixed to 2% of the critical damping. The raised floor is assumed to be extremely rigid in horizontal direction. The equipment is modeled as a SDOF system connected to the raised floor through a linear damper with damping coefficient c_e and a linear spring with lateral stiffness k_e as shown in Fig. 7.3. This stiffness can be modified to tune the equipment to different frequencies. The equipment damping is assumed to be equal to the structural damping to avoid the influence of non-classical damping in this study. The natural frequencies and effective modal masses of the fixed-base structures and the structure isolated by a suitably scaled RNC isolator (without equipment) are shown in Table 7.1.

To achieve effective isolation, it is necessary to increase the period of the isolated equipment to large values, which typically are larger than those required for effective isolation of buildings [115]. Accordingly, the equipment has a fundamental period of 0.0065 sec (in the case of relatively rigid equipment) and 8.546 sec in non-isolated and isolated conditions, respectively. The considered mass range of the equipment is 1% – 3% of the total mass of the structure (including the base mass).

7.5.1 Equations of motion

The following assumptions are made for the structural system under consideration: (1) the superstructure remains within the elastic limit during the earthquake excitation and the nonlinearity is concentrated only at the isolation elements; (2) the floors are assumed rigid in its own plane and the mass is lumped at each floor level; (3) the columns are inextensible and weightless providing the lateral stiffness; (4) the system is subjected to a single horizontal component of the earthquake ground motion; (5) the effects of soil–structure interaction are not taken into consideration.

The equations of motion for the fixed-base structure under earthquake ground acceleration are expressed in matrix form as

$$\mathbf{M}_\mathrm{s}\ddot{\mathbf{x}}_\mathrm{s} + \mathbf{C}_\mathrm{s}\dot{\mathbf{x}}_\mathrm{s} + \mathbf{K}_\mathrm{s}\mathbf{x}_\mathrm{s} = -\mathbf{M}_\mathrm{s}\mathbf{r}\ddot{x}_\mathrm{g}, \tag{7.2}$$

where $\mathbf{M}_\mathrm{s}$, $\mathbf{C}_\mathrm{s}$ and $\mathbf{K}_\mathrm{s}$ are the mass, damping and stiffness matrices of the superstructure, respectively; $\mathbf{x}_\mathrm{s} = \{x_1, x_2, \ldots, x_\mathrm{N}\}^T$, $\dot{\mathbf{x}}_\mathrm{s}$ and $\ddot{\mathbf{x}}_\mathrm{s}$ are the relative floor displacement, velocity and acceleration vectors, respectively; $\ddot{x}_\mathrm{g}$ is the earthquake ground acceleration; and $\mathbf{r}$ is the vector of influence coefficients. In the case of the isolated structure, the right-hand-side in the Eq. (7.2) is replaced by $-\mathbf{M}_\mathrm{s}\mathbf{r}(\ddot{x}_\mathrm{b} + \ddot{x}_\mathrm{g})$, where $\ddot{x}_\mathrm{b}$ is the relative acceleration of the base mass.

The corresponding equations of motion for the equipment and the isolated raised-floor mounted to a building floor under earthquake ground acceleration is expressed by

$$m_\mathrm{e}\,\ddot{x}_\mathrm{e} + c_\mathrm{e}\,\dot{x}_\mathrm{e} + k_\mathrm{e}\,x_\mathrm{e} = -m_\mathrm{e}\,(\ddot{x}_\mathrm{f} + \ddot{x}_\mathrm{r}) \tag{7.3}$$

$$m_\mathrm{r}\,\ddot{x}_\mathrm{r} - c_\mathrm{e}\,\dot{x}_\mathrm{e} - k_\mathrm{e}\,x_\mathrm{e} + \eta F_\mathrm{b} = -m_\mathrm{r}\,\ddot{x}_\mathrm{f} \tag{7.4}$$

where the subscript r denotes raised-floor; e refers to equipment; f denotes mounting floor and $\ddot{x}_\mathrm{f} = \ddot{x}_7 + \ddot{x}_\mathrm{g}$, where the 7th floor is the housing floor of the equipment. The restoring force developed in the isolation system of the raised floor F_b is modeled using the normalized Bouc-Wen hysteretic model in Eqs. (4.17)-(4.18).

In the case of the isolated structure, see Fig. 7.4(b), the corresponding equation of motion for the base mass under earthquake ground acceleration is expressed by

$$m_\mathrm{b}\,\ddot{x}_\mathrm{b} - c_1\,\dot{x}_1 - k_1\,x_1 + \eta F_\mathrm{b} = -m_\mathrm{b}\,\ddot{x}_\mathrm{g}, \tag{7.5}$$

where m_b and F_b are the base mass and the restoring force developed in the isolation system, respectively; c_1 and k_1 are the first story damping and stiffness, respectively; and η is the number of isolators. The restoring force F_b is expressed using the normalized Bouc-Wen model as

$$F_\mathrm{b}(t) = \kappa_x\,x_\mathrm{b}(t) + \kappa_w\,w(t), \tag{7.6}$$

$$\dot{w} = \rho(\dot{x}_\mathrm{b} - \sigma|\dot{x}_\mathrm{b}||w|^{n-1}w - (\sigma - 1)\dot{x}_\mathrm{b}|w|^n), \tag{7.7}$$

where κ_x, κ_w, ρ, σ and n are the shape controlling parameters of the hysteresis loop; $w(t)$ is an auxiliary variable which is not accessible to measurement and *dotw* denotes the time derivative. The lower value of the parameter σ is limited to $\frac{1}{2}$ and to guarantee BIBO stability, passivity, and consistency with physical asymptotic motion [200, 201].

7.5.2 Performance measures

The two main response quantities of interest in this chapter are: (1) the equipment absolute acceleration at its center of gravity (CG), which is a measure of the degree of protection; (2) the relative-to-floor equipment displacement, which quantifies the main side effect of equipment isolation.

7.5.3 Simulation tool

Having the input data given in Section 7.5 and the assumptions given in Section 5.5, the case study structure shown in Fig. 7.3 is modeled using the Structural Analysis Program SAP2000 *advanced* [6]. The proposed RNC isolator is modeled as a nonlinear support, whose dynamic behavior is governed by the hysteretic Bouc-Wen model, (7.6)–(7.7), where the rest of the structure is assumed to behave linearly. The parameters of the Bouc-Wen model have been identified, in Section 7.4.1. The mechanical characteristics of the RNC–c isolator are obtained in Section 7.3 and incorporated into the simulation code along with the isolator mass. Then the structural mass, stiffness and damping matrices are formed and related to other variables as shown explicitly by Eqs. (7.2)–(7.5). A modal analysis is performed first to determine the dynamic properties, of the modeled system, that are listed in Table 7.1. Then, a linear and nonlinear dynamic analysis are carried out in cases of fixed-base and isolated base structures, respectively, under a variety of ground motion excitations to determine the response quantities given in Section 7.5.2.

7.5.4 Displacement demand against isolator height

Practically, isolation of inner equipment necessitates isolators of relatively low profiles due to the limited storey heights. The RNC isolator offers adequate bearing capacity to support equipment. Therefore, its dimensions are mainly designed according to the displacement demand. One of the main parameters that control the RNC isolator rolling displacement is its height. A set of RNC isolators having the same mechanical characteristics, given in Section 7.3, but of different heights have been used in this study according to the displacement demand. The aim is to fulfill the displacement demand under various excitations but with the lowest possible isolator profile. Four displacement demands

of 0.11 m, 0.22 m, 0.33 m, 0.41 m have been considered and the corresponding total heights of the RNC isolators have been determined, being 0.28 m, 0.56 m, 0.76 m, 0.89 m, respectively. Other RNC isolators that provide higher displacement demands have been also used in this study, but they are not mentioned herein because their dimensions might be seen impractical for isolation of housed equipment.

7.6 Numerical assessment

Fig. 7.5 shows the response spectra of the ground accelerations and the $7th$ floor accelerations, at 2% structural damping ratio, when the fixed-base structure under study (cases I and III in Fig. 7.4(a and c)) is subjected to 6 selected earthquakes. Fig. 7.5 illustrates the amplification of the acceleration response in upper floors. Consequently, an equipment mounted on upper floors will be subjected to much stronger excitations than if it is mounted on lower floors.

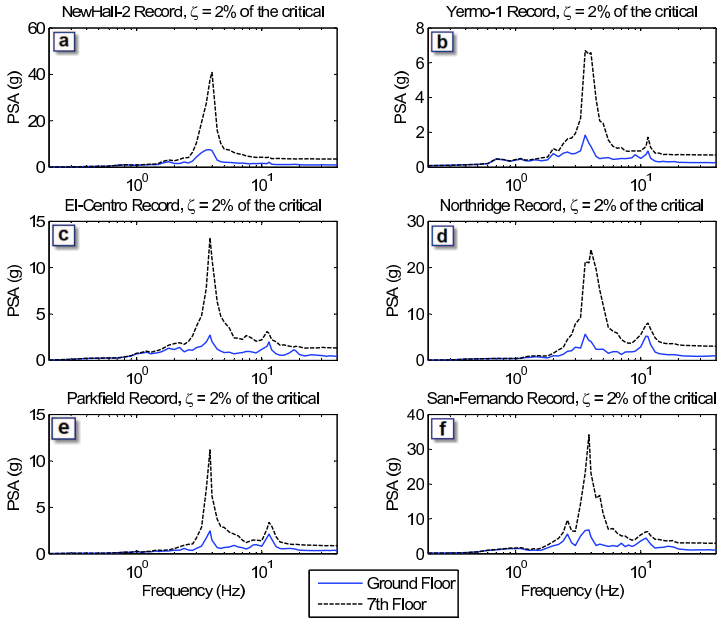

Figure 7.5: Response spectra for the ground and the $7th$ floor accelerations under the following earthquakes: (a) New-Hall 90°, (b) Yermo 0°, (c) El-Centro, (d) Northridge, (e) Parkfield, (f) San-Fernando. The structural damping ratio is 2% of the critical.

In this scenario, the purpose of this section is to analyze the efficiency of the RNC isolation device in reducing the acceleration of the equipment while keeping affordable displacements. This analysis is performed in two complementary

directions: (1) An example structure is subjected to a series of actual earthquakes; (2) The three example structures are subjected to constant-amplitude variable-frequency harmonic ground motions.

7.6.1 Actual earthquakes

The structure considered in this section has a lateral stiffness $\mathbf{K}_s$, and the three cases shown in Fig. 7.4 are analyzed. The dynamic properties of the structure for isolated and fixed-base conditions are given in Table 7.1. The equipment mass is taken as 3% of the total structural mass.

Fig. 7.6 displays the absolute acceleration time history of the equipment for the three cases under study (illustrated in Fig. 7.4) subjected to El-Centro earthquake. Fig. 7.7 displays the corresponding time history of the equipment displacement relative to the mounting building floor. It can be observed that the acceleration of the equipment is greatly reduced when comparing case I (fixed structure with RNC-isolated raised-floor) to case III (fixed structure with fixed equipment) in Fig. 7.6(b). This reduction is also significant when case I is compared to case II (isolated structure, using RNC isolator, with fixed equipment) in Fig. 7.6(a). Although cases I and II represent two approaches for equipment isolation, it is evident from Fig. 7.6(a) that the first approach is superior to the second one. Further, the former approach (case I) is expected to be more economic than the later one (case II). Fig. 7.7 shows that the associated displacement of the equipment in isolated cases I and II are larger than the displacement in the fixed case III, but they remain affordable. This emphasizes the ability of the proposed RNC isolator to greatly attenuate the equipment acceleration while keeping reasonable rolling displacement.

In Fig. 7.8, the effect of long-period ground excitations is considered using the Mexico-city earthquake. By comparing the dashed lines in both top and bottom plots in Fig. 7.8, it is observed that the acceleration response of case II is close to that of case III, i.e. isolation of the whole housing structure may not be the right decision to protect equipment under such excitation. On the other hand, the first approach (case I, represented by solid line in Fig. 7.8) reduces significantly the equipment acceleration response under the same long-period excitation.

Fig. 7.9 shows the peak absolute acceleration and relative displacement of the isolated (case I) and non-isolated (case III) equipment for eight selected earthquakes. Fig. 7.9(a) shows the general effectiveness of the proposed isolator in reducing a major part of the equipment acceleration. It is clear that the proposed system is capable of eliminating up to 98% of the equipment acceleration as for the Northridge earthquake, record number 6. This significant reduction is mainly due to the minimal base shear forces transmitted to the raised-floor through the RNC isolator. This is due to the great decoupling offered by: (i) The rolling concept upon which the RNC isolator is based on; (ii) The low

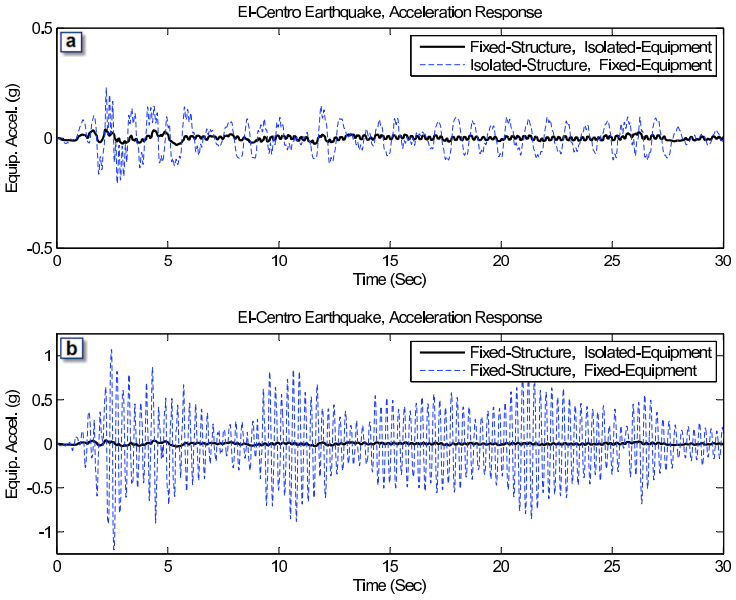

Figure 7.6: Absolute acceleration response time history of equipment under El-Centro earthquake: (a) Isolated-raised floor housed in a fixed-base structure vs fixed-base equipment housed in an isolated-base structure (*Case I* vs *Case II*), (b) Isolated-raised floor housed in a fixed-base structure vs fixed-base equipment housed in a fixed-base structure (*Case I* vs *Case III*).

post-yield stiffness of the designed RNC isolator, as characterized in Section 7.3. This decrease in acceleration is accompanied with some lateral displacement due to rolling. As shown in Fig. 7.9(b) these rolling displacements are in a reasonable range and seem to be small if compared to the overall structural dimensions. Indeed, the maximum rolling displacement of the isolated equipment corresponds to (record number 8) San Fernando earthquake (0.373 m) that contains strong motion at lower frequencies, which are close to that of the isolated equipment. However, the built-in recentering and damping mechanisms prevent permanent dislocation and allow for efficient restoration and motion damping. Moreover, the inherent buffer prevents undesirable excessive displacements in the lateral direction.

Further, the primary structures in cases I and III (Fig. 7.4) are excited by 36 actual earthquake ground motions to make sure that the good performance observed before can be achieved for a wider range of earthquake excitations. The displacement and acceleration responses of isolated versus non-isolated equipment are summarized in Table 7.2. Under a variety of ground motion excitations having different characteristics, the proposed RNC isolator shows significant efficiency in mitigating the equipment acceleration response while

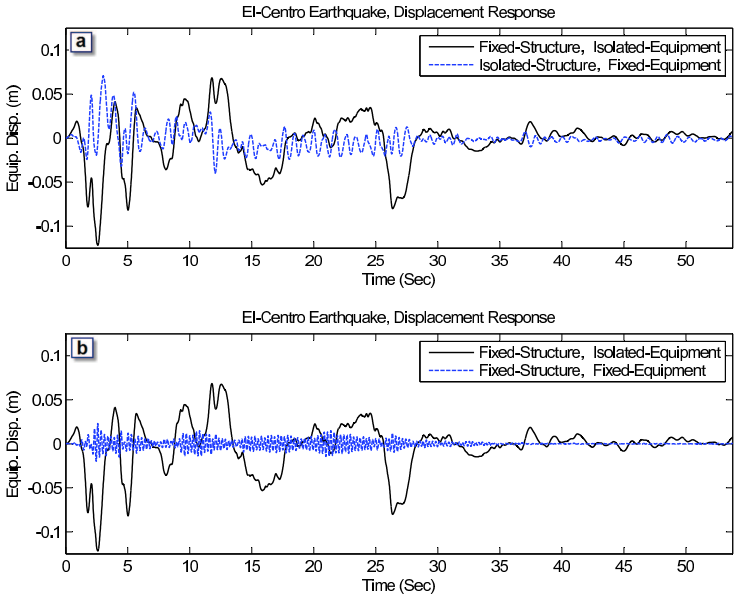

Figure 7.7: Time history of the equipment displacement relative to the mounting building floor under El-Centro earthquake: (a) Isolated-raised floor housed in a fixed-base structure vs fixed-base equipment housed in an isolated-base structure (*Case I* vs *Case II*), (b) Isolated-raised floor housed in a fixed-base structure vs fixed-base equipment housed in a fixed-base structure (*Case I* vs *Case III*).

exhibiting reasonable rolling displacement. Even under long-period excitations such as the Mexico-city earthquake, the RNC isolator still shows significant efficiency.

Regarding the displacement demand and the isolator height mentioned in Section 7.5.4, the results of Table 7.2 provide useful information for that purpose. The displacements of isolated equipment, sixth column from left in Table 7.2, are grouped with respect to the displacement demands of the four RNC isolators, mentioned in Section 7.5.4, as shown in Table 7.3. The third column from left in Table 7.3 gives the number of earthquakes that demand displacements that can be fulfilled by each isolator. From Table 7.3, it can be seen that a relatively low profile of 0.56 m can fulfill the displacement demands of up to 75% of the cases considered in Table 7.2, and up to 92% of the cases are within the capacity of the 0.76 m height RNC isolator.

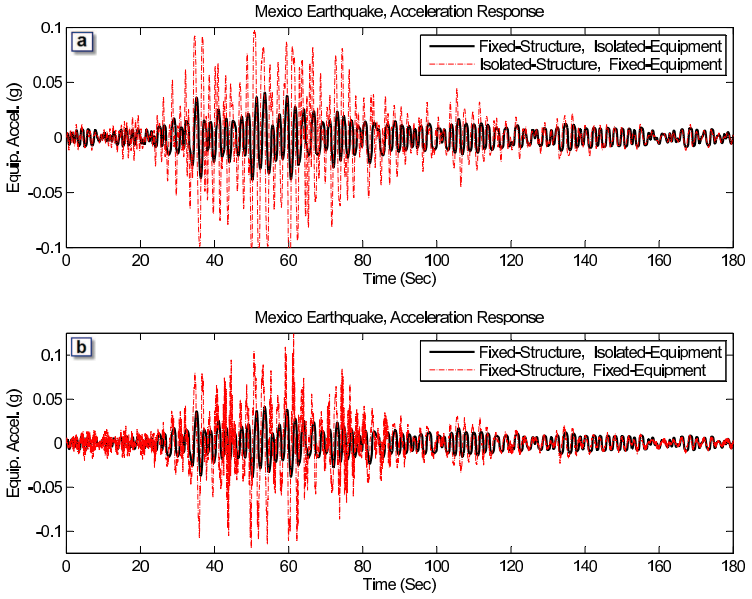

Figure 7.8: Absolute acceleration response time history of equipment under Mexico-city earthquake: (a) Isolated-raised floor housed in a fixed-base structure vs fixed-base equipment housed in an isolated-base structure (*Case I* vs *Case II*), (b) Isolated-raised floor housed in a fixed-base structure vs fixed-base equipment housed in a fixed-base structure (*Case I* vs *Case III*).

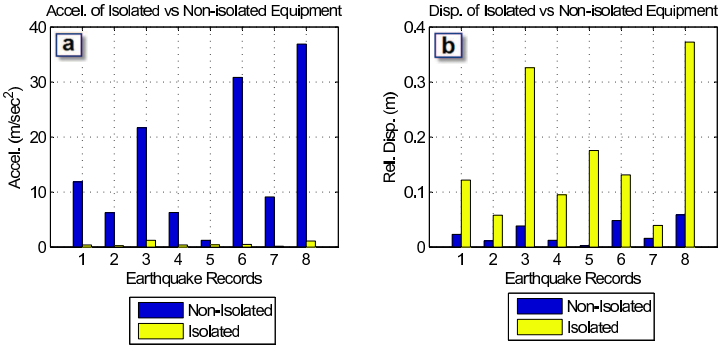

Figure 7.9: (a) Acceleration response of isolated vs non-isolated equipment for 8 earthquake records, (b) Isolated vs non-isolated associated relative displacement between the equipment and the housing 7th floor. The 8 earthquake records are: (1) El-Centro, (2) Kern, (3) Kobe, (4) Loma-Prieta, (5) Mexico, (6) Northridge, (7) Parkfield, (8) San-Fernando.

7.6.2 Harmonic excitations

To examine the effect of equipment mass and structural stiffness variations on the isolated equipment response, two equipment/structure mass ratios of 1% and 3% are used together with the three example structures having lateral stiffness $\frac{1}{2}\mathbf{K}_s$, $\mathbf{K}_s$ and $2\mathbf{K}_s$, whose dynamic properties are given in Table 7.1. Only cases I and III in Fig. 7.4 are considered in this analysis. The primary structures are subjected to different harmonic ground excitations with an amplitude $0.5g$ and different frequencies (f_g) ranging from 1.00 Hz to 40 Hz with an increment equal to 0.25 Hz.

Tables 7.4–7.6 give the peak values of the absolute acceleration and the relative displacement of the fixed-base and the isolated equipment for each case. By comparing the isolated an fixed-base cases in Tables 7.4–7.6, it is found that the proposed RNC isolation system is very effective in reducing the acceleration of the equipment even near the fundamental frequencies of the primary buildings, which are 2.86 Hz for $\frac{1}{2}\mathbf{K}_s$, 3.857 Hz for $\mathbf{K}_s$ and 5.104 Hz for $2\mathbf{K}_s$. In this study, the proposed isolator is designed to provide a great horizontal flexibility, which decreases acceleration significantly. However, this is associated with some lateral displacement on the rolling surface of the isolator. Except for a very low-frequency excitation (where the harmonic excitation frequency is close to that of the isolated equipment), these rolling displacements are within a reasonable range.

By comparing the results for 1% and 3% equipment/structure mass ratios in Tables 7.4–7.6, it is clear that increasing the equipment mass (reducing its frequency) increases the rolling displacement but reduces the equipment acceleration. On the other hand, the variation of the structural stiffness has a minimal influence on the response of the isolated equipment. This is due to the great decoupling of structure-equipment by means of the RNC isolator.

7.7 Conclusions

In this chapter, a reduced scale RNC–c isolator is designed, modeled, characterized and used for sensitive equipment isolation by means of a secondary raised floor, on which the equipment are mounted. The effectiveness of the RNC–c isolator is numerically investigated considering the case of equipment housed

in upper floors of a building, where the accelerations are amplified. Based on this investigation, the following conclusions can be drawn:

1. The RNC isolator is a robust isolation device and is very effective in controlling the response of motion-sensitive equipment for wide range of structural properties and earthquake characteristics.

2. The behavior of an equipment isolated by RNC isolator is relatively independent of the frequency content and the amplitude of base excitation.

3. From harmonic analysis, the results indicate that the RNC isolator is more effective in reducing the equipment acceleration response at the resonant frequency of the primary structure, while keeping the associated equipment motion below 0.30 m.

4. Under a series of 36 actual earthquakes, the maximum attained reduction in the peak absolute acceleration of equipment by the RNC isolator is 98% for many earthquakes, while the associated equipment-floor relative displacement is always below 0.375 m.

5. Under long-period ground motions like the Mexico City earthquake, the isolation of the entire housing structure is not the convenient approach to protect equipment, contrary to the RNC-isolated raised floor, which can eliminate up to 67% of the equipment acceleration.

6. Excluding the long period ground motions, the direct isolation of equipment via RNC-isolated raised floor system is far superior to the isolation of the entire housing structure using RNC isolators. Anyway, the equipment acceleration is significantly reduced using both approaches.

7. Increasing the isolated equipment mass (reducing its frequency) increases the rolling displacement but reduces the equipment acceleration. On the other hand, the variation of the structural stiffness has a minimal influence on the response of the isolated equipment. ■

	Mode Number								
	Isolator	1	2	3	4	5	6	7	8
Fixed-base Structure, Stiffness $= \frac{1}{2}K_s$									
Frequency (Hz)		2.860	8.472	13.762	18.535	22.614	25.860	28.184	29.557
Period (Sec)		0.350	0.118	0.073	0.054	0.044	0.039	0.035	0.034
Modal Participation Mass Ratios		0.858	0.091	0.029	0.013	0.006	0.003	0.000	0.000
Fixed-base Structure, Stiffness $= K_s$									
Frequency (Hz)		3.857	11.425	18.560	24.996	30.497	34.875	38.009	39.861
Period (Sec)		0.259	0.088	0.054	0.040	0.033	0.029	0.026	0.025
Modal Participation Mass Ratios		0.858	0.091	0.029	0.013	0.006	0.003	0.000	0.000
Fixed-base Structure, Stiffness $= 2K_s$									
Frequency (Hz)		5.104	15.118	24.56	33.076	40.355	46.148	50.295	52.745
Period (Sec)		0.196	0.066	0.041	0.030	0.025	0.022	0.020	0.019
Modal Participation Mass Ratios		0.858	0.091	0.029	0.013	0.006	0.003	0.000	0.000
Base-isolated Structure, Stiffness $= K_s$									
Frequency (Hz)	0.220	7.007	13.837	20.301	26.171	31.223	35.266	38.174	39.900
Period (Sec)	4.552	0.143	0.072	0.049	0.038	0.032	0.028	0.026	0.025
Modal Participation Mass Ratios	0.999	0.001	0.000	0.000	0.000	0.000	0.000	0.000	0.000

Table 7.1: Modal properties of example structures without equipment.

Equipment/Structure mass ratio = 1% and Structure's lateral stiffness = K_s							
	Earthquake		**Non-Isolated equipment**		**Isolated equipment**		Reduction
No.	Record	Peak Accel. (g)	Rel. Disp. (m)	Peak Accel. (m/sec^2)	Rel. Disp. (m)	Peak Accel. (m/sec^2)	(%)
1	ALTADENA 0°	0.448	0.0292	15.8977	0.0420	0.3299	98%
2	ALTADENA 90°	0.179	0.0071	4.2643	0.0084	0.1332	97%
3	ARRAY06 0°	0.376	0.0202	11.2952	0.3049	0.6873	94%
4	ARRAY06 90°	0.437	0.0262	15.0973	0.5764	1.0516	93%
5	CORRALIT 0°	0.630	0.0521	28.3104	0.0946	0.5913	98%
6	CORRALIT 90°	0.479	0.0255	15.0698	0.1657	0.4749	97%
7	HOLLISTE 0°	0.369	0.0144	7.7122	0.1985	0.6898	91%
8	HOLLISTE 90°	0.178	0.0168	9.3717	0.1640	0.3360	96%
9	LACC-NOR 0°	0.222	0.0106	5.6443	0.0678	0.2995	95%
10	LACC-NOR 90°	0.256	0.0246	13.2492	0.0615	0.2506	98%
11	LEXINGT 0°	0.442	0.0162	8.7660	0.2068	0.8117	91%
12	LEXINGT 90°	0.410	0.0216	11.6343	0.3161	0.9803	92%
13	LUCERNE 0°	0.681	0.0081	11.8413	0.1139	0.4093	97%
14	LUCERNE 90°	0.703	0.0275	19.9379	0.1089	0.3524	98%
15	NEW-HALL 0°	0.590	0.0589	32.7304	0.2893	0.8273	97%
16	NEW-HALL 90°	0.583	0.0656	36.1720	0.2005	0.6164	98%
17	OAK-WHAF 0°	0.287	0.0109	5.7637	0.0896	0.4594	92%
18	OAK-WHAF 90°	0.271	0.0131	6.8429	0.1043	0.4266	94%
19	PETROLIA 0°	0.590	0.0209	12.3905	0.1315	0.5591	95%
20	PETROLIA 90°	0.662	0.0241	13.9574	0.3127	0.9619	93%
21	POMONA 0°	0.186	0.0151	9.3387	0.0150	0.1619	98%
22	POMONA 90°	0.207	0.0098	6.4272	0.0148	0.1517	98%
23	SANTA-MONICA 0°	0.370	0.0180	10.8338	0.0773	0.2874	97%
24	SANTA-MONICA 90°	0.883	0.0480	30.8220	0.1311	0.4690	98%
25	SYLMAR 0°	0.843	0.0454	25.1010	0.4107	1.2574	95%
26	SYLMAR 90°	0.604	0.0206	11.0541	0.2044	0.7543	93%
27	YERMO 0°	0.151	0.0143	7.9039	0.1530	0.3247	96%
28	YERMO 90°	0.245	0.0137	7.1296	0.2973	0.4596	94%
29	EL-CENTRO	0.348	0.0231	11.8343	0.1218	0.3900	97%
30	KERN	0.179	0.0112	6.2217	0.0578	0.2296	96%
31	KOBE	0.679	0.0384	21.6752	0.3260	1.2067	94%
32	LOMA-PRIETA	0.276	0.0121	6.2564	0.0950	0.3893	94%
33	MEXICO	0.100	0.0025	1.2171	0.1755	0.4006	67%
34	NORTHRIDGE	0.883	0.0480	30.8216	0.1312	0.4691	98%
35	PARKFIELD	0.237	0.0157	9.1186	0.0393	0.1510	98%
36	SAN-FERNANDO	1.171	0.0584	36.9040	0.3725	1.1073	97%

Table 7.2: Response summary under 36 seismic excitations.

Isolator height (m)	Equipment rel. disp. (m)	Number of valid cases / Total cases	Percentage (%)
0.28	≤ 0.11	14 / 36	39 %
0.56	≤ 0.22	27 / 36	75 %
0.76	≤ 0.33	33 / 36	92 %
0.89	≤ 0.41	35 / 36	97 %
The rest	≥ 0.41	1 / 36	3 %

Table 7.3: Displacement demands against the RNC isolator heights.

Structure's lateral stiffness = $\frac{1}{2}K_s$										
Excitation Frequency	Equipment/Structure mass ratio = 1%				Accel. Reduction	Equipment/Structure mass ratio = 3%				Accel. Reduction
	Fixed-base Equipment		Isolated Equipment			Fixed-base Equipment		Isolated Equipment		
(Hz)	Disp. (m)	Accel. (m/sec^2)	Disp. (m)	Accel. (m/sec^2)	%	Disp. (m)	Accel. (m/sec^2)	Disp. (m)	Accel. (m/sec^2)	%
1.00	0.0218	5.7158	0.5972	1.3484	76%	0.0227	5.7499	0.7073	1.2181	79%
1.25	0.0238	6.3358	0.4653	1.1065	83%	0.0248	6.4027	0.5372	1.0044	84%
1.50	0.0283	7.6696	0.3709	0.9337	88%	0.0298	7.8115	0.4439	0.8525	89%
1.75	0.0354	9.8299	0.3105	0.8056	92%	0.0370	9.9509	0.3682	0.7399	93%
2.00	0.0393	11.0541	0.2707	0.7092	94%	0.0423	11.5336	0.3208	0.6543	94%
2.25	0.0567	16.3808	0.2342	0.6353	96%	0.0634	17.7387	0.2807	0.5872	97%
2.50	0.0946	28.0780	0.2109	0.5772	98%	0.1141	32.8317	0.2521	0.5335	98%
2.75	0.3309	101.4019	0.1899	0.5302	99%	0.3409	101.3864	0.2265	0.4895	99%
3.00	0.1223	38.7161	0.1709	0.4917	99%	0.1040	31.9310	0.2068	0.4527	99%
5.00	0.0096	4.5741	0.0899	0.3099	93%	0.0094	4.4019	0.1145	0.2690	94%
10.00	0.0003	3.6885	0.0382	0.1979	95%	0.0004	3.3774	0.0450	0.1599	95%
20.00	0.0004	1.5278	0.0119	0.1298	92%	0.0004	1.6405	0.0137	0.0941	94%
30.00	0.0047	3.2032	0.0058	0.1067	97%	0.0042	2.9928	0.0066	0.0721	98%
40.00	0.0023	3.6659	0.0037	0.0941	97%	0.0023	3.0882	0.0040	0.0605	98%

Table 7.4: The frequency of harmonic base excitations vs equipment displacement and acceleration responses, at Equipment/Structure mass ratios of 1% and 3%. The structure's lateral stiffness = $\frac{1}{2}K_s$.

Structure's lateral stiffness = K_s										
Excitation	Equipment/Structure mass ratio = 1%				Accel.	Equipment/Structure mass ratio = 3%				Accel.
Frequency	Fixed-base Equipment		Isolated Equipment		Reduction	Fixed-base Equipment		Isolated Equipment		Reduction
(Hz)	Disp. (m)	Accel. (m/sec^2)	Disp. (m)	Accel. (m/sec^2)	%	Disp. (m)	Accel. (m/sec^2)	Disp. (m)	Accel. (m/sec^2)	%
1.00	0.0112	5.3041	0.5943	1.3425	75%	0.0116	5.3198	0.7056	1.2153	77%
1.25	0.0117	5.5847	0.4651	1.1002	80%	0.0122	5.6133	0.5381	1.0024	82%
1.50	0.0130	6.3306	0.3657	0.9374	85%	0.0134	6.3807	0.4400	0.8552	87%
1.75	0.0151	7.3773	0.3084	0.8163	89%	0.0160	7.5719	0.3655	0.7454	90%
2.00	0.0146	7.1680	0.2708	0.7224	90%	0.0153	7.2847	0.3211	0.6605	91%
2.25	0.0170	8.4929	0.2310	0.6478	92%	0.0180	8.6994	0.2780	0.5929	93%
2.50	0.0188	9.4981	0.2087	0.5878	94%	0.0200	9.8071	0.2503	0.5383	95%
2.75	0.0274	14.1328	0.1879	0.5390	96%	0.0296	14.7626	0.2247	0.4934	97%
3.00	0.0337	17.6190	0.1704	0.4987	97%	0.0381	19.3891	0.2061	0.4559	98%
4.00	0.0779	44.7036	0.1261	0.3901	99%	0.0620	34.5002	0.1522	0.3524	99%
5.00	0.0143	9.2390	0.0952	0.3209	97%	0.0136	8.5542	0.1166	0.2867	97%
10.00	0.0031	7.3222	0.0378	0.1993	97%	0.0032	7.6626	0.0448	0.1605	98%
20.00	0.0004	1.9403	0.0116	0.1304	93%	0.0004	1.8249	0.0136	0.0950	95%
30.00	0.0021	4.8775	0.0056	0.1072	98%	0.0024	4.9283	0.0065	0.0726	99%
40.00	0.0030	2.9941	0.0035	0.0944	97%	0.0026	2.7371	0.0039	0.0608	98%

Table 7.5: The frequency of harmonic base excitations vs equipment displacement and acceleration responses, at Equipment/Structure mass ratios of 1% and 3%. The structure's lateral stiffness = K_s.

Structure's lateral stiffness = $2K_s$										
Excitation	Equipment/Structure mass ratio = 1%				Accel.	Equipment/Structure mass ratio = 3%				Accel.
Frequency	Fixed-base Equipment		Isolated Equipment		Reduction	Fixed-base Equipment		Isolated Equipment		Reduction
(Hz)	Disp. (m)	Accel. (m/sec^2)	Disp. (m)	Accel. (m/sec^2)	%	Disp. (m)	Accel. (m/sec^2)	Disp. (m)	Accel. (m/sec^2)	%
1.00	0.0062	5.1243	0.5932	1.3424	74%	0.0064	5.1330	0.7049	1.2156	76%
1.25	0.0064	5.2671	0.4630	1.0990	79%	0.0066	5.2818	0.5364	1.0017	81%
1.50	0.0067	5.6149	0.3652	0.9324	83%	0.0070	5.6033	0.4391	0.8531	85%
1.75	0.0075	6.3565	0.3093	0.8138	87%	0.0079	6.4922	0.3667	0.7447	89%
2.00	0.0071	5.9897	0.2651	0.7241	88%	0.0074	6.0375	0.3173	0.6617	89%
2.25	0.0079	6.7135	0.2285	0.6527	90%	0.0082	6.7710	0.2757	0.5955	91%
2.50	0.0080	6.8331	0.2088	0.5944	91%	0.0084	6.9284	0.2503	0.5415	92%
2.75	0.0110	9.6210	0.1859	0.5459	94%	0.0111	9.3593	0.2229	0.4966	95%
3.00	0.0111	9.6926	0.1671	0.5052	95%	0.0121	10.3069	0.2037	0.4589	96%
5.00	0.1537	150.8902	0.0993	0.3280	99%	0.1037	98.7376	0.1204	0.2908	99%
10.00	0.0023	4.2021	0.0381	0.1975	95%	0.0023	4.0885	0.0439	0.1598	96%
20.00	0.0001	2.5963	0.0109	0.1314	95%	0.0002	2.4491	0.0133	0.0955	96%
30.00	0.0014	4.9829	0.0055	0.1071	98%	0.0011	4.5857	0.0064	0.0726	98%
40.00	0.0013	4.0980	0.0034	0.0936	98%	0.0013	4.2444	0.0039	0.0608	99%

Table 7.6: The frequency of harmonic base excitations vs equipment displacement and acceleration responses, at Equipment/Structure mass ratios of 1% and 3%. The structure's lateral stiffness = $2K_s$.

8

Equipment isolation: isolated structure approach

8.1 Introduction

The recent history reveals that strong earthquakes can cause some badly designed structures or buildings to fail or collapse, and also cause some well-designed structures to malfunction due to the damage or failure of the equipment housed in the structure or building. Both the failure of structures and equipment can cause serious harm to the residents or personnel working in a building. In this context, seismic isolation has been proven to be an effective means for protecting the structures and attached equipment [482].

A number of research works have been conducted by implementing isolation systems at the base of the equipment-structure system, aiming to reduce the earthquake forces transmitted from the ground. Based on a theoretical and experimental investigation, [250] showed that seismic protection can be achieved effectively for lightweight equipment mounted on structure isolated with elastic bearings at the base. A hybrid isolation system with base-isolated floors was proposed by [205] for protection of highly sensitive devices mounted on a structure subjected to support motions. Considering the effects of torsion and translation, [485] studied the seismic response of light equipment mounted on torsional buildings supported by elastic bearings. The results indicated that the response of an equipment structure system can be effectively reduced through installation of base isolators, and there exists an optimal location for mounting the equipment.

Considering the use of sliding bearings [63, 177], the response of an equipment attached to a sliding primary structure under earthquake excitations was

investigated in [487, 302, 483, 486, 9]. The results showed that the response of equipment can be effectively reduced through the installation of sliding support at the structural base, in comparison with that of a structure with fixed base. Experimental results for secondary systems mounted on a sliding base-isolated structure [230] concluded that the acceleration response of the secondary system may be amplified when the input motions are composed of low-frequency vibrations. In this case, the sliding bearings are not considered to be an effective isolation device, which implies that the base-isolated structure is not suitable for a construction site with soft soil.

Recently, the problem of building isolation has received more attention than ever due to the construction of high-precision factories worldwide. More and more stringent requirements have been employed in this regard for removing the ambient or man-made vibrations [371, 415]. To allow sensitive equipment to operate in a harsh environment, [444] proposed an optimization procedure for the design of vibration isolators aimed at minimizing the response of the internal components of electronic equipment. As for protection of high-tech equipment from micro- or ambient vibrations, [477] showed that passive hybrid floor isolation systems are more effective in mitigating the equipment response than passive or hybrid base isolation systems. [469, 488] studied the response of a batch of high-tech equipment mounted on a hybrid platform, which in turn is mounted on a building floor.

In this chapter, the RNC–c isolator is adopted to isolate structures containing sensitive equipment, that are directly rested on the building floor, i.e. fixed-base equipment. The efficiency of the RNC–c isolator is numerically evaluated considering the case of equipment housed in upper floors of a building, where the accelerations are amplified and the motion contains strong components at long periods. Such case studies are presented in Section 8.5 and the corresponding results are given in Section 8.6.

8.2 The used RNC isolator type

In this chapter, the RNC–c isolator is designed to isolate structures equipped with motion sensitive equipment on upper floors. The RNC–c isolator type is shown in Fig. 3.1. For the designed RNC–c isolator, the horizontal and vertical distances between the furthermost points are 2.48 m and 1.40 m, respectively. The isolator dimensions are chosen to allow for a 53 cm as a maximum rolling displacement, beyond which the buffer mechanism stops the isolated structure with minimal shock.

8.3 Mechanical characteristics

Following the mechanical characterization scheme described in Section 4.2, the designed RNC–c isolator used in this chapter, to isolate building structures, has the following mechanical characteristics:

- Maximum vertical load capacity = 600 kN.
- Pre-yield stiffness = 6816.84 kN m^{-1}.
- Post-yield stiffness = 410.15 kN m^{-1}.
- Yield displacement = 1.29 cm.
- Yield force = 95.50 kN.

Further, and to draw relatively general conclusions about the performance of the RNC–c isolator, four different designs of the RNC–c isolator,, ranging from very stiff (sets I) to very flexible (sets IV) designs, are evaluated in this study. The maximum vertical load capacity per bearing is 600 kN. Table 8.1 gives the basic mechanical characteristics of such designs. These characteristics have been also obtained following the scheme given in Section 4.2.

Isolator Set	Isolator Period (T_b)	Elastic Stiffness (k_e)	Post-yield Stiffness (k_b)	Yield Strength (f_y)	Characteristic Strength (Q)
I	2.211 sec	13633.68	820.31	193.01	190.50
II	3.118 sec	6816.84	410.15	96.50	95.25
III	4.404 sec	3408.42	205.10	48.25	47.62
IV	6.224 sec	1704.20	102.55	24.13	23.81

Table 8.1: Characteristics of different isolator sets used in this study, kN-m units.

8.4 Hysteretic modeling

The characterization described in Chapter 4 has shown that the RNC isolator exhibits a hysteretic behavior that is potentially described by the Bouc-Wen model, as shown in Fig. 4.7. The objective of this section is to obtain an input-output mathematical model to describe in a reasonable and manageable form the force-displacement relationship exhibited by the RNC–c isolator using the Bouc-Wen model of smooth hysteresis, described in Section 4.5. The normalized form of the Bouc-Wen model is used in this chapter. Such form of the model is defined in Section 4.5.4.

8.4.1 Bouc-Wen model parameters estimation

The normalized Bouc-Wen form provides an exact and explicit expression for the hysteretic limit cycle [200, 199]. Moreover, by using a periodic input signal $x(t)$ along with the analytic description of the limit cycle, a robust parametric nonlinear, nonrecursive identification method was presented in [201, 194]. This method is used in this chapter. For identification, the ANSYS code characterization described in Section 4.2 is used as the "true" isolator device. A periodic input horizontal displacement $x(t)$ is applied at the lowermost surface and the "measured" force is obtained at the topmost surface of the RNC isolator.

The values of the identified parameters of the normalized Bouc-Wen are:

$$\kappa_{\mathrm{x}} = 19.3147;\ \kappa_{\mathrm{w}} = 16.2265;\ \rho = 55.6406;\ \sigma = 1.0223;\ n = 2.1618$$

These values guarantee that the model is consistent with basic physical properties such as bounded-input bounded-output (BIBO) stability and energy dissipation [199].

In Fig. 8.1, the measured output restoring force of the isolator is plotted against the calculated one via the identified normalized Bouc-Wen model. The good matching supports the accuracy of the Bouc-Wen model to capture the nonlinear hysteretic behavior of the RNC isolator.

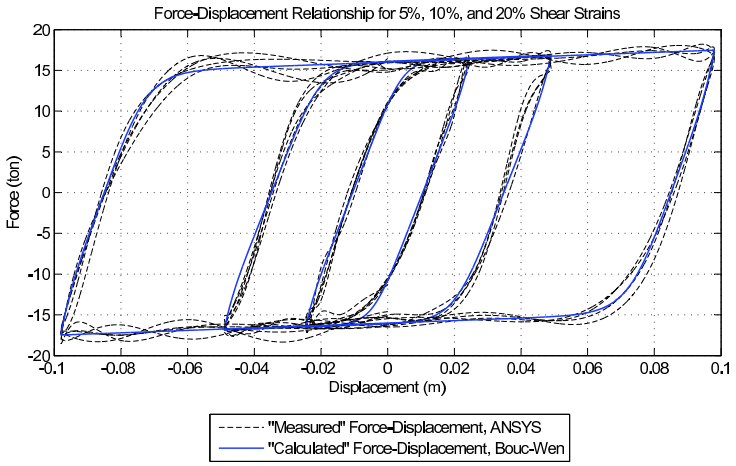

Figure 8.1: Measured vs calculated restoring force for 5%, 10%, and 20% shear strains.

8.4.2 Seismic verification of the Bouc-Wen model

To check the validity of the identified parameters, both periodic and actual random seismic displacement (El-Centro) input signals are input into the AN-

SYS and the Bouc-Wen model. Then, the discrepancy between the measured and predicted outputs, F_{m} and F_{b}, is quantified using the L_1 and L_∞-norms and the corresponding relative errors ε:

$$||f||_1 = \int_0^{T_e} |f(t)|\,\mathrm{d}\,t\,; \quad ||f||_\infty = \max_{t\in[0,T_e]} |f(t)|\,; \quad \varepsilon_{1,\infty} = \frac{||F_{\mathrm{m}} - F_{\mathrm{b}}||_{1,\infty}}{||F_{\mathrm{m}}||_{1,\infty}}\,. \tag{8.1}$$

The relative error ε_1 quantifies the ratio of the bounded area between the output curves to the area of the measured force along the excitation duration T_e, while ε_∞ measures the relative deviation of the peak force.

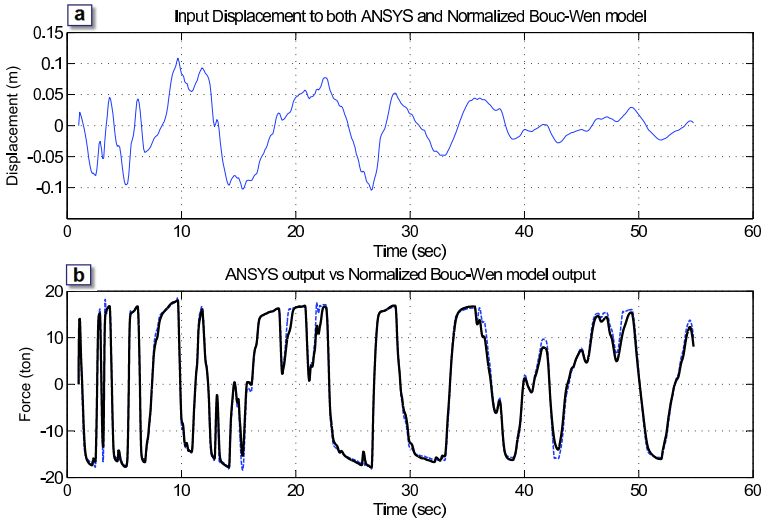

Figure 8.2: (a) Input displacement of El-Centro earthquake to ANSYS and the Bouc-Wen model, (b) Measured (ANSYS) output vs calculated (Bouc-Wen model) output, the relative error $\varepsilon_1 = 5.70\%$ and $\varepsilon_\infty = 3.15\%$, respectively. ANSYS Output (- - -), Bouc-Wen Model Output (——).

Fig. 8.2(a) shows the input displacement of El-Centro earthquake record. The measured restoring force from ANSYS is plotted against the predicted one using Bouc-Wen model in Fig. 8.2(b). As can be seen, there is a close match of both measured and predicted output curves with a relatively small error. Hence, the Bouc-Wen model can be considered a good practical mathematical description of the proposed RNC isolator for further analysis.

8.5 Implementation

The remaining of the chapter is devoted to the implementation of the RNC device to isolate a building structure that houses equipment. The scenario

shown in Fig. 8.3 is considered as a case study. The equipment is attached to the 7th floor of a primary eight-story building structure. As equipment mounted to upper floors are subjected to much stronger excitation than if they are mounted to lower floors, this can be considered as the worst case to evaluate the effectiveness of the RNC isolator. For comparison purposes, two cases are studied as illustrated in Fig. 8.3: (a) RNC-isolated structure-equipment, and (b) fixed-base structure-equipment. This section presents the main tools for the numerical evaluation, while Section 8.6 will describe and analyze the results.

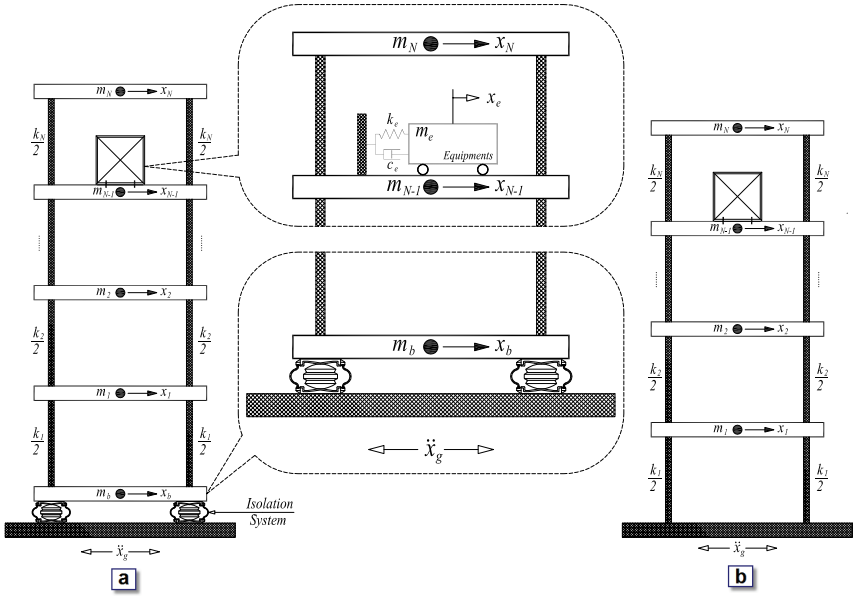

Figure 8.3: Idealized structure-equipment system, (a) RNC-Isolated-base structure, (b) Fixed-base structure.

The supporting structure is chosen as an eight-stories reinforced concrete moment resisting frame modeled as a shear building, where all significant vibrational modes, the structure-equipment-interaction, and the isolator nonlinearities are included in the performed analysis in order to get more realistic results. The assumptions given in Section 5.5 are also valid for the structural system under consideration in this chapter. The cross sectional dimensions of the frame columns and beams are 1.0×0.25 m and 0.70×0.25 m, respectively. All the stories are 3.0 m height and the frame span is 5.0 m centerline-to-centerline. The frame material is normal-weight concrete with a total material volume per frame of 19 m^3. This concrete material has the following isotropic properties:

- Weight per unit volume = 23563.12 N m^{-3}
- Mass per unit volume = 2402.77 Kg m^{-3}
- Modulus of elasticity = 2.486E+10 N m^{-2}

- Poisson's ratio = 0.20
- Shear modulus = 1.036E+10 N m^{-2}
- Specified concrete compressive strength = 27579032 N m^{-2}

The structural damping ratio for all modes is fixed to 2% of the critical damping. The equipment is modeled as a SDOF mounted directly to the $7th$ floor through a linear damper (with coefficient c_e) and a linear spring with lateral stiffness k_e, which is modified to tune the equipment frequency to different structural modal frequencies. The equipment damping is assumed to be equal to the structural damping. The natural frequencies and effective modal mass of the fixed-base structure and the structure isolated by an RNC isolator (without equipment) are shown in Table 8.2. The considered mass of the equipment is 1% of the total mass of the structure (including the base mass).

8.5.1 Equations of motion

The following assumptions are made for the structural system under consideration: (1) the superstructure remains within the elastic limit during the earthquake excitation and the nonlinearity is concentrated only at the isolation elements; (2) the floors are assumed rigid in its own plane and the mass is lumped at each floor level; (3) the columns are inextensible and weightless providing the lateral stiffness; (4) the system is subjected to single horizontal component of the earthquake ground motion; (5) the effects of soil–structure interaction are neglected. The equations of motion for fixed-base structure under earthquake ground acceleration are expressed as

$$\mathbf{M}_s\ddot{\mathbf{x}}_s + \mathbf{C}_s\dot{\mathbf{x}}_s + \mathbf{K}_s\mathbf{x}_s = -\mathbf{M}_s\mathbf{r}\ddot{x}_g, \tag{8.2}$$

where $\mathbf{M}_s$, $\mathbf{C}_s$ and $\mathbf{K}_s$ are the mass, damping, and stiffness matrices of the superstructure, respectively; $\mathbf{x}_s = \{x_1, x_2, \ldots, x_N\}^T$, $\dot{\mathbf{x}}_s$ and $\ddot{\mathbf{x}}_s$ the unknown relative floor displacement, velocity and acceleration vectors, respectively; $\ddot{x}_g$ is the earthquake ground acceleration; and $\mathbf{r}$ is the vector of influence coefficients.

In the case of isolated structure, see Fig. 8.3(a), the right-hand-side in the Eq. (8.2) is replaced with $-\mathbf{M}_s\mathbf{r}(\ddot{x}_b + \ddot{x}_g)$, where $\ddot{x}_b$ is the relative acceleration of the base mass. The corresponding equation of motion for the base mass under earthquake ground acceleration is expressed by

$$m_b\,\ddot{x}_b - c_1\,\dot{x}_1 - k_1\,x_1 + \eta F_b = -m_b\,\ddot{x}_g, \tag{8.3}$$

where m_b and F_b are the base mass and the restoring force developed in the isolation system, respectively; c_1 and k_1 are the first story damping and stiffness, respectively; and η is the number of isolators. The restoring force F_b

developed in the isolation system is modeled using the normalized Bouc-Wen model as

$$F_{\mathrm{b}}(t) = \kappa_x \, x_{\mathrm{b}}(t) + \kappa_w \, w(t), \tag{8.4}$$

$$\dot{w} = \rho(\dot{x}_{\mathrm{b}} - \sigma|\dot{x}_{\mathrm{b}}||w|^{n-1}w - (\sigma - 1)\dot{x}_{\mathrm{b}}|w|^{n}), \tag{8.5}$$

where κ_x, κ_w, ρ, σ and n are the shape controlling parameters of the hysteresis loop; $w(t)$ is an auxiliary variable which is not accessible to measurement and *dotw* denotes the time derivative. The lower value of the parameter σ is limited to $\frac{1}{2}$ and to guarantee BIBO stability, passivity, and consistency with physical asymptotic motion [200, 201].

8.5.2 Structure equipment interaction

For light secondary systems mounted on heavier primary structures, it is well known that the response of the light secondary system is affected by four major dynamic characteristics [190, 191, 192, 484]. The first issue is the *tuning*, which means that the natural frequency of the equipment is coincident with that of the structure. Such an effect may amplify the response of the equipment due to the fact that the light secondary system behaves as if it were a vibration absorber of the heavier primary system. The second issue is *interaction*, which is related to the feedback effect between the motion of the primary and secondary systems. Ignoring this effect may result in an overestimation of the true response of the secondary system. The third issue is the *non-classical damping*, which may occur when the damping properties of the two systems are drastically different, such that the natural frequencies and mode shapes of the combined system can only be expressed in terms of complex numbers. The last issue is *spatial coupling*, which relates to the effect of multiple support motions when the secondary system of interest is mounted at multiple locations.

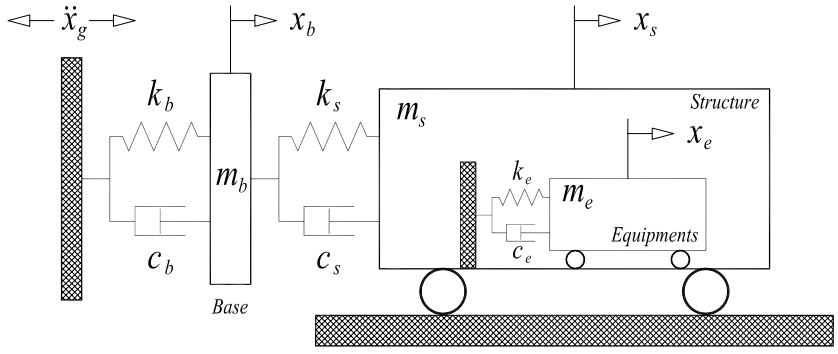

Figure 8.4: Model of an isolated structure-equipment system.

In this section we seek a simple relation between the fundamental frequency of an isolated building and the equipment frequency. This relation may help to specify a limit that separates two cases: (i) miss-tuned equipment (the equipment response is amplified); and (ii) properly tuned equipment (the equipment response is not amplified). To simplify the analysis, we consider (see Fig. 8.4) a model of a simplified base-isolated structure-equipment system with a purely linear isolator, with the following equation of motion:

$$\begin{Bmatrix} m_\mathrm{e}\ddot{x}_\mathrm{e} \\ m_\mathrm{s}\ddot{x}_\mathrm{s} \\ m_\mathrm{b}\ddot{x}_\mathrm{b} \end{Bmatrix} + \begin{bmatrix} c_\mathrm{e} & -c_\mathrm{e} & 0 \\ -c_\mathrm{e} & c_\mathrm{s}+c_\mathrm{e} & -c_\mathrm{s} \\ 0 & -c_\mathrm{s} & c_\mathrm{s}+c_\mathrm{b} \end{bmatrix} \begin{Bmatrix} \dot{x}_\mathrm{e} \\ \dot{x}_\mathrm{s} \\ \dot{x}_\mathrm{b} \end{Bmatrix} + \begin{bmatrix} k_\mathrm{e} & -k_\mathrm{e} & 0 \\ -k_\mathrm{e} & k_\mathrm{s}+k_\mathrm{e} & -k_\mathrm{s} \\ 0 & -k_\mathrm{s} & k_\mathrm{s}+k_\mathrm{b} \end{bmatrix} \begin{Bmatrix} x_\mathrm{e} \\ x_\mathrm{s} \\ x_\mathrm{b} \end{Bmatrix} = -\begin{Bmatrix} m_\mathrm{e} \\ m_\mathrm{s} \\ m_\mathrm{b} \end{Bmatrix} \ddot{x}_\mathrm{g} \tag{8.6}$$

where m, c and k represent mass, damping coefficient and stiffness, respectively. The subscripts e, s and b are associated with the DOF of equipment, structure and base, respectively; x is the relative-to-ground displacement; and $\ddot{x}_\mathrm{g}$ is the ground acceleration.

By neglecting damping and assuming harmonic ground displacement, $x_\mathrm{g} = X_\mathrm{g}\mathrm{e}^{i\omega t}$, where X_g is the amplitude and ω is the excitation frequency, a closed-form solution is sought herein to examine the key parameters involved in the considered problem. After long symbolic manipulation, the steady-state absolute acceleration responses of the structure and equipment can be expressed as

$$\ddot{x}_\mathrm{s} = \frac{k_\mathrm{b}\ddot{x}_\mathrm{g}}{D(\omega)} \tag{8.7a}$$

$$\ddot{x}_\mathrm{e} = \frac{k_\mathrm{b}\ddot{x}_\mathrm{g}}{(1-f_\mathrm{e}^2)D(\omega)} \tag{8.7b}$$

where

$$D(\omega) = (k_\mathrm{b} - m_\mathrm{b}\omega^2) - (1 + \frac{k_\mathrm{b}}{k_\mathrm{s}} - \varepsilon_\mathrm{b} f_\mathrm{s}^2)\left(m_\mathrm{s} + \frac{m_\mathrm{e}}{1-f_\mathrm{e}^2}\right)\omega^2 \tag{8.8}$$

in which $\varepsilon_\mathrm{b} = m_\mathrm{b}/m_\mathrm{s}$ is the mass ratio, $f_\mathrm{e} = \omega/\omega_\mathrm{e}$, and $f_\mathrm{s} = \omega/\omega_\mathrm{s}$. When considering the effect of resonance between equipment and excitation, i.e. $\omega_\mathrm{e} = \omega$ where ω is the excitation frequency, the acceleration responses of the system in Eqs. (8.7a)–(8.7b) become

$$\ddot{x}_\mathrm{s} = 0 \tag{8.9a}$$

$$\ddot{x}_\mathrm{e} = \frac{-k_\mathrm{b}\ddot{x}_\mathrm{g}}{k_\mathrm{e}[1 + (k_\mathrm{b} - m_\mathrm{b}\omega_\mathrm{e}^2)/k_\mathrm{s}]} \tag{8.9b}$$

Because of the coincidence of the ground excitation frequency with the equipment frequency, the equipment behaves like a vibration absorber of the structure. For this reason, the response of the equipment is greatly amplified,

as implied by Eq. (8.9b). Further, let us consider the case when the structural frequency is equal to the equipment frequency, that is, $\omega_e = \omega_s = \omega$. For this case, the responses of the system in Eqs. (8.7a)–(8.7b) can be approximated as

$$\ddot{x}_s \approx 0 \tag{8.10a}$$

$$\ddot{x}_e \approx \frac{-k_b \ddot{x}_g}{\varepsilon_e[k_s(1-\varepsilon_b)+k_b]} \tag{8.10b}$$

This indicates that the acceleration response of the equipment may be more amplified, as implied by the relatively small mass ratio ($\varepsilon_e = m_e/m_s$) and large stiffness ratio (k_b/k_s) in Eq. (8.10b).

In this dissertation, the first priority is to reduce the vibrations of the equipment, rather than the structure. So, by comparing the denominators in Eqs. (8.7a) and (8.7b), one may observe that the condition $|1 - f_e^2| \geq 1$ or $f_e = \omega/\omega_e \geq \sqrt{2}$ has to be fulfilled. It can be shown that this is equivalent to the following condition:

$$\frac{\omega_e}{\omega_s} \leq \sqrt{\frac{k_b/k_s}{2[1+(m_b+m_e)/m_s]}} \tag{8.11}$$

Since the fundamental frequency ω_s of a base-isolated structure is generally low in practice, the horizontal stiffness of the equipment attached to the structure must be designed to be soft enough to satisfy such condition for the sake of vibration reduction.

To extend the condition (8.11) to the case of multi-degree of freedom structure (MDOF) shown in Fig. 8.3(a), we consider only the fundamental (isolator) frequency (ω_1) of the isolated structure-equipment system, which is approximated as $\omega_1 \approx \sqrt{k_b/(m_e+m_s+m_b)}$ because the mode shape is governed mainly by the isolator flexibility and the superstructure exhibits almost a rigid body motion. After some manipulations, Eq. (8.11) becomes

$$\frac{\omega_e}{\omega_1} \leq \sqrt{\frac{m_e+m_s+m_b}{4m_e+2m_s+4m_b}} \tag{8.12}$$

This expression has been obtained under some simplifications, but it will be used in this chapter under more realistic conditions, considering damping, seismic excitation and the nonlinear RNC isolator.

8.5.3 Performance measures

The main three response quantities of interest in this chapter are: (1) the equipment absolute acceleration at its center of gravity (CG), which is a measure

of the degree of protection; (2) the relative-to-ground base (bearing) displacement, which is crucial in the design of isolation systems; (3) structural absolute acceleration at the topmost floor, which represents the main source of damaging housed sensitive equipment.

8.5.4 Simulation tool

Having the input data given in Section 8.5 and the assumptions given in Section 5.5, the case study structure shown in Fig. 8.3 is modeled using the Structural Analysis Program SAP2000 *advanced* [6]. The proposed RNC isolator is modeled as a nonlinear support, whose dynamic behavior is governed by the hysteretic Bouc-Wen model, (8.4)–(8.5), where the rest of the structure is assumed to behave linearly. The parameters of the Bouc-Wen model have been identified, in Section 8.4.1. The mechanical characteristics of the RNC–c isolator are obtained in Section 8.3 and incorporated into the simulation code along with the isolator mass. Then the structural mass, stiffness and damping matrices are formed and related to other variables as shown explicitly by Eqs. (8.2)–(8.3). A modal analysis is performed first to determine the dynamic properties, of the modeled system, that are listed in Table 8.2. Then, a linear and nonlinear dynamic analysis are carried out in cases of fixed-base and isolated base structures, respectively, under a variety of ground motion excitations to determine the response quantities given in Section 8.5.3.

8.6 Response of structure–equipment systems

Fig. 8.5 shows the response spectra of the ground accelerations and the $7th$ floor accelerations, at 2% structural damping ratio, when the fixed-base structure under study is subjected to 6 selected earthquakes. Fig. 8.5 illustrates the amplification of the acceleration response in upper floors. Consequently, an equipment mounted on upper floors will be subjected to much stronger excitations than if it is mounted on lower floors.

In this context, the purpose of this section is twofold: (1) to demonstrate the effectiveness of the RNC isolator to reduce the seismic response of the structure-equipment system shown in Fig. 8.3; (2) to evaluate the robustness of the RNC isolator under variations of

- Equipment frequency,
- Isolator mechanical properties,
- Structural vibration period,
- Ground motion characteristics.

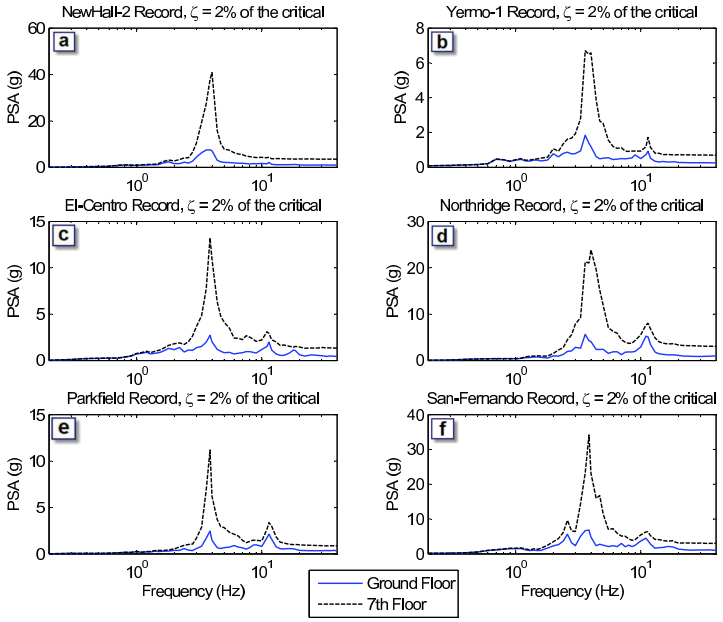

Figure 8.5: Response spectra for the ground and the $7th$ floor accelerations under the following earthquakes: (a) New-Hall 90°, (b) Yermo 0°, (c) El-Centro, (d) Northridge, (e) Parkfield, (f) San-Fernando. The structural damping ratio is 2% of the critical.

Since our main objective is to to mitigate the equipment acceleration response and, moreover, to keep it lower than that of the structure, the equipment frequency (ω_e) should fulfill the inequality (8.12). In such a case, the equipment is said to be properly tuned. In this study, three tuning conditions are considered:

1. Properly-tuned equipment with $\omega_e = \frac{1}{5}\omega_1$,

2. Miss-tuned equipment with $\omega_e = 5\omega_1$,

3. Miss-tuned equipment with $\omega_e = \omega_1$ and $\omega_e = \omega_2$ in the case of fixed-base and isolated structure-equipment systems, respectively. This represents the most severe condition of equipment tuning in both cases.

As for ground motions, two excitation types are considered: (i) constant-amplitude variable-frequency harmonic excitations; and (ii) a wide variety of actual earthquakes. The results are presented and discussed in the next two subsections.

8.6.1 Harmonic excitations

In this section, four different designs of the RNC isolator (see Table 8.1) are evaluated with the aim of choosing an appropriate one for the rest of this study. This evaluation is based on exciting the structure-equipment system by a harmonic input, which is defined as a sinusoidal ground acceleration

$$\ddot{x}_{\mathrm{g}}(t) = 0.5g \sin(2\pi f_{\mathrm{g}} t) \tag{8.13}$$

where f_{g} denotes the excitation frequency and g is the gravitational acceleration. The harmonic excitation frequency is 1 Hz.

Fig. 8.6 shows the maximum equipment acceleration as a function of the structural fundamental frequency, using the four RNC isolator designs and considering two equipment tuning conditions: properly tuned ($\omega_{\mathrm{e}} = \frac{1}{5}\omega_1$) and miss-tuned ($\omega_{\mathrm{e}} = 5\omega_1$) equipment. In all cases, the equipment response in a fixed-base structure is included for comparison.

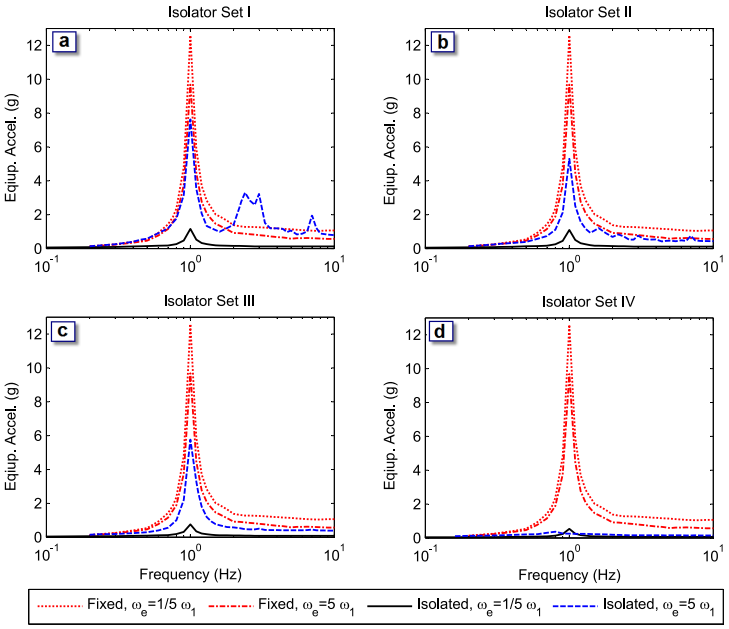

Figure 8.6: Maximum equipment acceleration versus structural fundamental frequency for properly and miss-tuned equipment frequency: (a) Isolator set I, (b) Isolator set II, (c) Isolator set III, (d) Isolator set IV.

From the first glance, it can be observed that all the RNC designs are effective in reducing the equipment acceleration as compared to the fixed-base

cases. Particularly, when the equipment is properly tuned, the response reduction is much more significant (solid lines in Fig. 8.6). It can be interesting to see how miss-tuning deteriorates the equipment acceleration response for the different RNC isolators. During base excitation, the isolator performance is mainly governed by the post-yield stiffness k_{b}, that is provided by the metallic yield dampers after exceeding the yield limit. For the highest value of k_{b}, isolator I in Fig. 8.6(a), the response deterioration is maximum. This negative effect diminishes gradually as k_{b} decreases, as shown in Figs. 8.6(b,c). For very low value of k_{b}, isolator IV Fig. 8.6(d), the effect of miss-tuning is practically suppressed.

On the other hand, lower pre-yield stiffness renders the isolator highly sensitive to minor vibrations. Considering that the wind loads represent the source of minor vibrations, the example structure in Fig. 8.3 has been subjected to a wind pressure of 2 kN m^{-2} including suction. Although the details are omitted here, it has been found that the RNC isolator II (see Table 8.1) fulfills the minimum requirements to resist these loads. Consequently, softer designs III and IV are discarded.

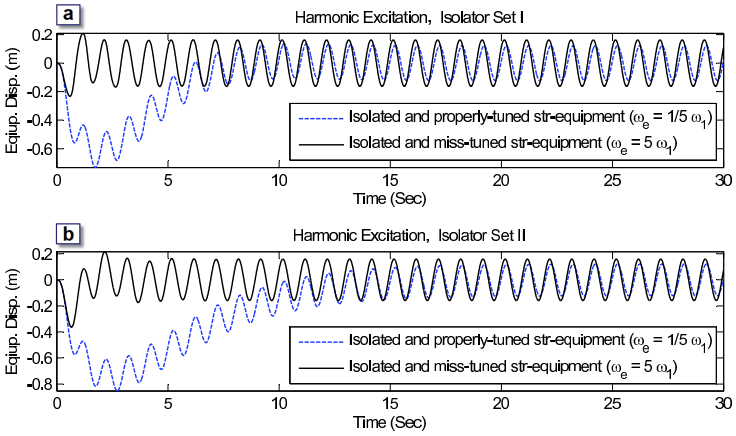

Figure 8.7: Harmonic equipment displacement time history for the two equipment tuning frequencies using: (a) Isolator set I, (b) Isolator set II.

Fig. 8.7 displays the equipment displacement time history using the RNC isolator designs I and II under the harmonic ground motion. It can be observed that the equipment displacement quickly reaches the steady-state within the first few cycles, specially for miss-tuned equipment. Meanwhile, softer design II exhibits larger transient displacement and takes longer time to reach the steady-state, with a slightly lower vibration amplitude. In both cases, there is no permanent displacement before the steady-state response is reached. Certainly, this highlights the efficiency of the gravity-based restoring mechanism, which

is an inherent characteristic of the proposed RNC isolator.

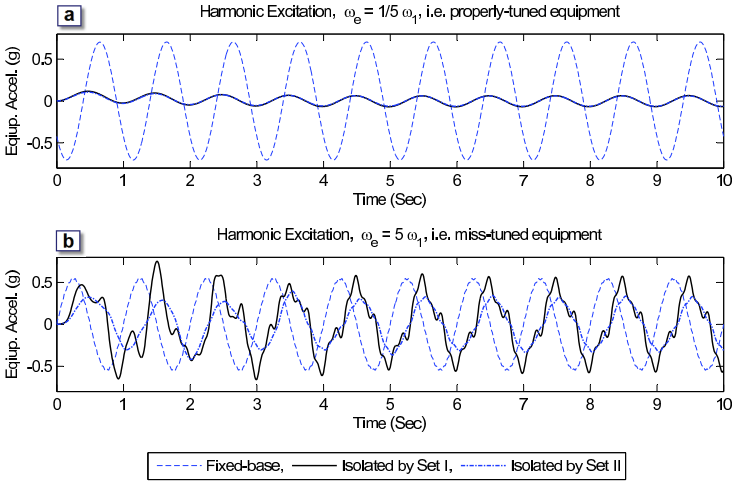

Figure 8.8: Equipment acceleration time history under harmonic excitation using isolators I and II for: (a) Properly-tuned equipment, (b) Miss-tuned equipment.

Fig. 8.8 plots the equipment absolute acceleration under the same excitation. Fig. 8.8(a) illustrates that both designs I and II give the same response reduction, relative to the fixed-base case, and shows clearly the vibration period of 1 second. In the miss-tuning case, Fig. 8.8(b), the acceleration response is contaminated with higher modal frequencies, particularly for the stiffer isolator I. For the softer design II, the steady-state response is achieved in a faster way, accompanied by a larger reduction on equipment acceleration. This supports the selection of isolator set II for further study, considering actual earthquakes as a more realistic excitation.

8.6.2 Actual earthquakes

The formulations of the tuning effect on equipment response in Section 8.5.2 have been made by neglecting the damping of the structural system and by assuming harmonic ground motion. In practice, there is always some damping associated with the structural system, while the ground motion may be random in nature.

Fig. 8.9 presents the equipment absolute acceleration response in RNC-isolated and fixed-base structures under El Centro earthquake. Two equipment frequencies are considered: properly tuned ($\omega_e = 1/5\omega_1$) and miss-tuned ($\omega_e = 5\omega_1$) based on Eq. (8.12). From this figure, the following observations can be made: (1) Comparing the fixed-base equipment responses in Figs. 8.9(a)

and 8.9(b), proper tuning of equipment reduces its acceleration response; (2) Comparing the isolated and fixed-base in Fig. 8.9(a), the RNC isolator along with proper tuning reduces very significantly the equipment acceleration. The same comparison in Figs 8.9(b) shows that the RNC isolator is still effective when the equipment is miss-tuned.

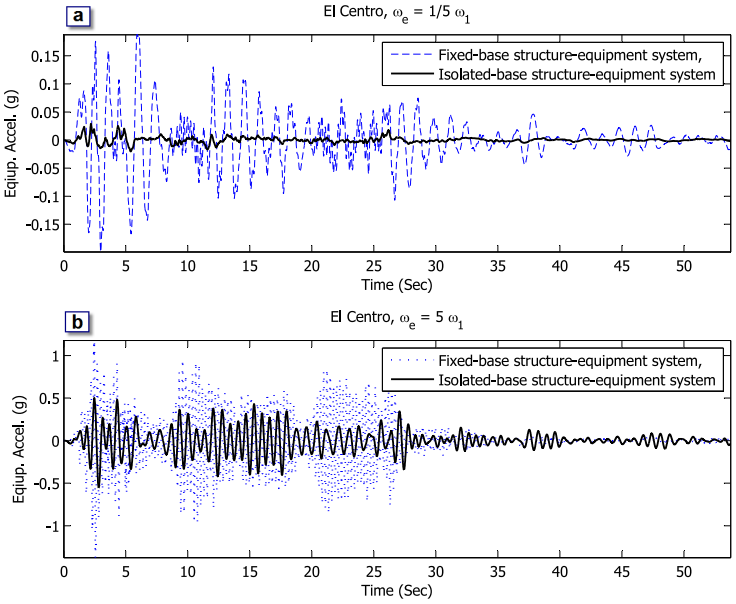

Figure 8.9: Acceleration response time history of equipment, under El Centro earthquake, using different tuning frequencies: (a) Properly-tuned equipment, (b) Miss-tuned equipment.

To further examine the performance of the RNC isolator, sets of numerical experiments are performed considering three issues: (a) A wide range of structures having fundamental vibration periods within the range 0.10 – 1.50 sec; (b) Five different ground motion records that range from very low to very severe intensity, their peak ground accelerations PGAs range from $0.18g$ – $1.17g$; (c) Two equipment tuning frequencies (properly tuned ($\omega_e = 1/5\omega_1$) and miss-tuned ($\omega_e = 5\omega_1$)). The peak equipment accelerations of fixed-base and base-isolated structure-equipment systems are listed in Table 8.3. The response quantities of interest are:

1. $\ddot{x}_{e-F}$, equipment acceleration in a fixed-base structure, where the equipment is properly-tuned,

2. $\ddot{x}_{e-P}$, equipment acceleration in a RNC-isolated structure, where the equipment is properly-tuned,

3. $\ddot{x}_{e-M}$, equipment acceleration in a RNC-isolated structure, where the equipment is miss-tuned.

From Table 8.3, it is apparent that the RNC isolator, together with a proper equipment tuning, is greatly effective in reducing the equipment absolute acceleration under all earthquakes and structural periods considered. Indeed, the ratio $\ddot{x}_{e-P}/\ddot{x}_{e-F}$ of the peak acceleration in the isolated, properly tuned case to that of the fixed-base case is always around 8 %. In this case, proper tuning of equipment housed in an isolated-base structure works as a second filter of vibration in series with the main isolation system (first filter) of the whole structure. The resultant of the two filters approaches an isolation bearing of equipment with very low resistance to motion, which translates into great equipment decoupling from the vibrating base. As a consequence, a great attenuation of equipment response is attained when it is mounted to a wide range of structures, even those structures having large time period.

Comparing the isolated miss-tuned responses with the fixed base case in Table 8.3, it is observed that the RNC isolator reduces the response effectively within some range of structural periods. This range is relatively narrow under lower intensity earthquakes (e.g. 0.30 – 1.00 sec under Kern earthquake of PGA=0.18g) and enlarges under higher intensity earthquakes, where the RNC isolator is effective for all periods (e.g. 0.10 – 1.50 sec under San Fernando earthquake of PGA=1.17g). Further, within each range, the isolator efficiency is maximum at the structural period for which the fixed-base case gives the maximum peak equipment acceleration.

Regarding the usefulness of the proposed RNC isolator under long-period ground motions, the Mexico City 1985 earthquake has been used as an excitation for fixed-base and isolated-base structure-equipment system. The equipment absolute acceleration time histories are shown in Fig. 8.10(a). It is clear that the proposed RNC isolator can be functional under such type of earthquake ground motions, as it could attenuate up to 83% of the equipment acceleration response for properly tuned equipment, but at the expense of larger equipment displacement as illustrated by Fig. 8.10(b). On the other hand, the equipment miss-tuning does amplify its acceleration and displacement responses as shown in Fig. 8.10(c). This emphasizes the significance of equipment tuning under such earthquakes.

To better assess the efficiency of the RNC isolator under different earthquakes having distinctive characteristics, a series of 36 actual ground motions have been utilized to excite fixed-base and isolated-base structure-equipment

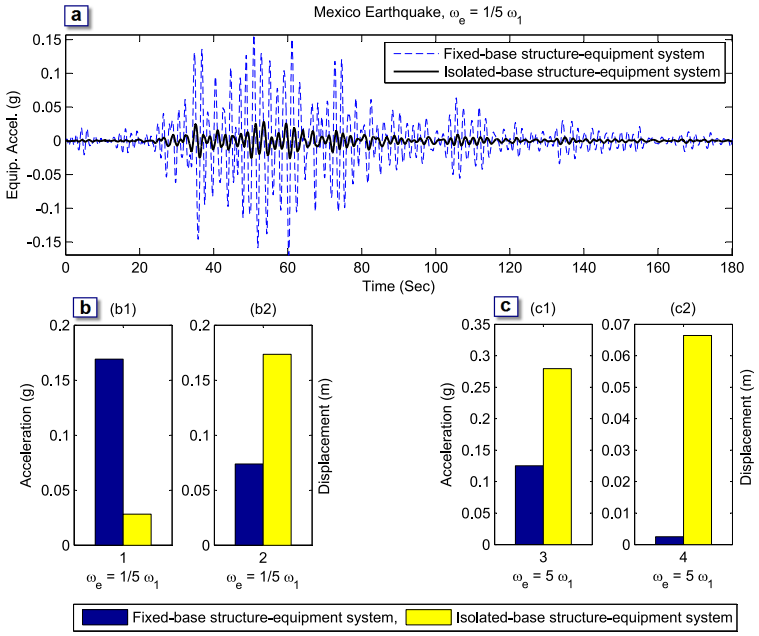

Figure 8.10: (a) Acceleration time history of equipment under the long-period Mexico-city earthquake, where the equipment is properly tuned to the structure i.e. $\omega_e = \frac{1}{5}\omega_1$, (b) Acceleration and displacement peak responses under Mexico-city earthquake, when the equipment is properly tuned, i.e. $\omega_e = \frac{1}{5}\omega_1$, (c) The same when the equipment is miss-tuned, i.e. $\omega_e = 5\omega_1$

systems. The equipment frequency is set to the most severe tuning condition. It is tuned to first and second vibration modes in the case of fixed-base and RNC-isolated structure-equipment systems, respectively. The isolated base drift and absolute accelerations of structure and equipment in both cases are listed in Table 8.4. Two main observations can be drawn from Table 8.4:

1. Except for Mexico earthquake, the RNC isolator mitigates substantially both the equipment and the structural absolute accelerations, while keeping affordable base displacement, for the rest of the considered base excitations. This means that the RNC isolator exhibits a robust behavior under a wide variety of ground motions.

2. The reduction of the equipment acceleration response is relatively higher than that of the structure, under the same excitation, which is the main objective of this study. This is specially apparent in the case of the long-period Mexico earthquake. In this case, the RNC isolator has almost a neutral effect on the structural response, but it achieves up to 59%

reduction in the equipment absolute acceleration. This reduction has been attained in a real challengeable case, which involves a long-period ground motion plus an equipment under the most severe tuning condition.

8.7 Conclusions

In chapter 7, a reduced scale RNC–c isolator is designed, modeled, characterized and used for sensitive equipment isolation by means of a secondary raised floor, on which the equipment are mounted, where the structure itself is mainly fixed-based. In this chapter, the RNC–c isolator is adopted to isolate structures containing sensitive equipment, that are directly rested on the building floor, i.e. fixed-base equipment and isolated structure. The efficiency of the RNC–c isolator is numerically assessed considering the case of equipment housed in upper floors of a building, where the accelerations are amplified and the motion contains strong components at long periods. Three variables have been chosen as performance measures: base displacement (base drift), structural acceleration and equipment acceleration. Based on numerical results, the following conclusions can be drawn:

1. The proposed RNC isolator is a very efficient tool for equipment seismic protection via isolation of the entire housing structure.

2. The RNC isolator exhibits a robust behavior under a very wide range of structural vibration periods and ground motions including long-period earthquakes.

3. Proper tuning of equipment enhances more the RNC isolator performance.

4. The negative effect of equipment miss-tuning diminishes with the increase of the RNC isolator flexibility and the earthquake intensity.

5. The isolator efficiency is maximum at the structural period for which the fixed-base case gives the maximum peak equipment acceleration.

6. The RNC isolator efficiency increases as its yield strength decreases.

7. The RNC isolator has an efficient inherent gravity-based re-centering mechanism.

8. The period of the RNC isolator increases with the decrease of yield strength of the metallic yield dampers and the increase of its flexibility. ■

	Mode Number								
		1	2	3	4	5	6	7	8
Fixed-base Structure									
Frequency (Hz)		3.857	11.425	18.560	24.996	30.497	34.875	38.009	39.861
Period (Sec)		0.259	0.088	0.054	0.040	0.033	0.029	0.026	0.025
Effective Modal Mass (%)		0.858	0.091	0.029	0.013	0.006	0.003	0.000	0.000
	Mode Number								
	Isolator (1)	2	3	4	5	6	7	8	9
Base-isolated Structure									
Isolator Set II									
Frequency (Hz)	0.321	7.029	13.846	20.306	26.174	31.224	35.266	38.174	39.900
Period (Sec)	3.118	0.142	0.072	0.049	0.038	0.032	0.028	0.026	0.025
Effective Modal Mass (%)	0.999	0.001	0.000	0.000	0.000	0.000	0.000	0.000	0.000

Table 8.2: Modal properties of fixed-base and isolated structure without equipment.

T_s	KERN, PGA=0.18g			PARKFIELD, PGA=0.24g			EL CENTRO, PGA=0.35g			KOBE, PGA=0.68g			SAN FERNANDO, PGA=1.17g		
	Fixed-b. str.	Isolated-b. str.		Fixed-b. str.	Isolated-b. str.		Fixed-b. str.	Isolated-b. str.		Fixed-b. str.	Isolated-b. str.		Fixed-b. str.	Isolated-b. str.	
(sec)	$\ddot{x}_{e-F}$	$\ddot{x}_{e-P}$	$\ddot{x}_{e-M}$	$\ddot{x}_{e-F}$	$\ddot{x}_{e-P}$	$\ddot{x}_{e-M}$	$\ddot{x}_{e-F}$	$\ddot{x}_{e-P}$	$\ddot{x}_{e-M}$	$\ddot{x}_{e-F}$	$\ddot{x}_{e-P}$	$\ddot{x}_{e-M}$	$\ddot{x}_{e-F}$	$\ddot{x}_{e-P}$	$\ddot{x}_{e-M}$
0.10	2.829	0.142	3.617	1.747	0.085	2.211	7.819	0.283	4.685	9.846	0.945	3.461	6.611	0.840	4.409
0.20	2.966	0.142	3.576	2.085	0.085	2.098	8.661	0.283	4.740	11.224	0.945	3.535	8.671	0.840	4.489
0.30	4.216	0.142	3.502	3.342	0.085	1.987	10.410	0.283	4.835	12.818	0.945	3.680	15.554	0.840	4.685
0.40	6.333	0.141	3.415	4.456	0.085	2.155	14.862	0.282	4.890	24.671	0.944	3.575	32.956	0.839	4.707
0.50	8.898	0.141	3.562	6.247	0.084	2.122	26.604	0.283	5.501	27.165	0.946	4.594	37.083	0.840	5.617
0.60	11.940	0.140	3.294	8.087	0.084	2.256	30.096	0.283	5.722	35.482	0.941	4.788	27.976	0.837	6.284
0.70	10.763	0.140	3.397	6.929	0.082	2.306	24.873	0.283	6.240	32.423	0.940	5.542	22.308	0.837	6.984
0.80	8.110	0.139	3.503	4.979	0.081	2.281	19.269	0.282	6.950	27.677	0.944	8.244	18.715	0.837	7.364
0.90	6.142	0.139	3.425	3.309	0.081	2.156	14.431	0.282	7.715	26.363	0.953	10.879	21.949	0.838	7.793
1.00	4.347	0.138	3.447	3.148	0.080	2.646	10.381	0.283	8.491	27.719	0.944	9.919	21.044	0.839	8.325
1.10	3.753	0.137	3.384	2.363	0.082	2.471	9.781	0.285	9.201	26.654	0.942	10.508	18.079	0.840	8.728
1.20	3.404	0.136	3.347	2.639	0.083	2.355	9.190	0.288	9.575	29.917	0.937	8.989	16.444	0.838	8.947
1.30	3.888	0.104	3.268	2.421	0.084	2.337	8.995	0.290	9.810	27.308	0.935	8.190	16.186	0.837	9.070
1.40	3.273	0.134	3.443	2.144	0.086	2.392	9.101	0.293	9.864	21.520	0.928	8.785	15.810	0.835	9.102
1.50	3.060	0.133	3.978	1.941	0.086	2.604	9.254	0.295	9.617	16.995	0.920	9.973	14.862	0.831	8.936

Table 8.3: Effects of structural time period on RNC isolator efficiency under different tuning conditions and seismic excitations, utilizing the RNC isolator set II. Accelerations are in (m/sec^2).

	Earthquake		Base drift	Structural acceleration		Reduction	Equipment acceleration		Reduction
No.	Record	Peak Accel. (g)	(m)	**Fixed**	**Isolated**	(%)	**Fixed**	**Isolated**	(%)
1	ALTADENA 0°	0.448	0.044	14.03	2.32	83%	52.10	7.11	86%
2	ALTADENA 90°	0.179	0.014	4.40	0.85	81%	13.66	2.67	80%
3	ARRAY06 0°	0.376	0.149	8.03	1.75	78%	34.91	4.08	88%
4	ARRAY06 90°	0.437	0.244	9.61	2.13	78%	59.91	3.28	95%
5	CORRALIT 0°	0.63	0.100	23.34	2.90	88%	116.01	5.56	95%
6	CORRALIT 90°	0.479	0.101	12.14	2.25	81%	52.53	4.66	91%
7	HOLLISTE 0°	0.369	0.194	6.93	2.51	64%	26.06	7.30	72%
8	HOLLISTE 90°	0.178	0.051	5.50	1.42	74%	34.32	2.24	93%
9	LACC-NOR 0°	0.222	0.051	7.85	1.51	81%	27.73	2.90	90%
10	LACC-NOR 90°	0.256	0.036	9.95	1.49	85%	57.89	2.45	96%
11	LEXINGT 0°	0.442	0.155	7.66	2.30	70%	20.52	6.92	66%
12	LEXINGT 90°	0.410	0.174	6.97	2.17	69%	45.49	5.89	87%
13	LUCERNE 0°	0.681	0.061	20.34	1.85	91%	16.04	3.45	78%
14	LUCERNE 90°	0.703	0.040	25.12	1.75	93%	65.35	4.46	93%
15	NEW-HALL 0°	0.590	0.218	19.88	3.05	85%	107.93	9.73	91%
16	NEW-HALL 90°	0.583	0.103	25.70	2.83	89%	151.66	9.43	94%
17	OAK-WHAF 0°	0.287	0.093	5.73	1.71	70%	18.88	3.98	79%
18	OAK-WHAF 90°	0.271	0.130	4.94	2.02	59%	19.73	5.37	73%
19	PETROLIA 0°	0.590	0.116	12.23	2.54	79%	59.03	7.93	87%
20	PETROLIA 90°	0.662	0.279	10.43	2.65	75%	54.58	8.15	85%
21	POMONA 0°	0.186	0.021	6.68	1.15	83%	33.88	2.21	93%
22	POMONA 90°	0.207	0.017	5.22	1.05	80%	23.40	2.63	89%
23	SANTA-MONICA 0°	0.370	0.041	10.23	1.46	86%	36.13	3.72	90%
24	SANTA-MONICA 90°	0.883	0.088	34.38	2.29	93%	142.27	6.29	96%
25	SYLMAR 0°	0.843	0.284	23.38	2.95	87%	60.95	8.99	85%
26	SYLMAR 90°	0.604	0.187	10.82	2.64	76%	38.53	6.95	82%
27	YERMO 0°	0.151	0.047	7.03	1.19	83%	33.36	2.09	94%
28	YERMO 90°	0.245	0.097	5.08	1.51	70%	20.07	2.81	86%
29	EL-CENTRO	0.348	0.061	9.92	2.24	77%	47.13	5.68	88%
30	KERN	0.179	0.032	4.85	1.36	72%	25.63	1.95	92%
31	KOBE	0.679	0.410	17.98	3.64	80%	68.87	8.36	88%
32	LOMA-PRIETA	0.276	0.085	4.90	2.05	58%	15.74	4.62	71%
33	MEXICO	0.100	0.048	1.16	1.10	5 %	2.80	1.14	59%
34	NORTHRIDGE	0.883	0.088	34.38	2.29	93%	142.27	6.28	96%
35	PARKFIELD	0.237	0.021	6.37	1.02	84%	26.78	2.02	92%
36	SAN-FERNANDO	1.171	0.301	25.78	2.94	89%	107.28	8.31	92%

Table 8.4: Response summary under 36 seismic excitations and the most severe equipment tuning conditions. The equipment is tuned to 1st and 2nd modes in the case of fixed-base and isolated structure-equipment systems, respectively, RNC–c set II. Accelerations are in m/sec^2.